Mathematical Models and Methods in Applied Sciences
Vol. 27, No. 11 (2017) 1993–2030

DOI: 10.1142/S0218202517500373

Numerical approximations for a three-component Cahn–Hilliard phase-field model based on the invariant energy quadratization method

Xiaofeng Yang*
Department of Mathematics, University of South Carolina, Columbia, SC 29208, USA
xfyang@math.sc.edu

Jia Zhao*
Department of Mathematics, University of South Carolina, Columbia, SC 29208, USA
Department of Mathematics, University of North Carolina, Chapel Hill, NC 29599, USA
zhaojia@email.unc.edu

Qi Wang
School of Materials Science and Engineering, Nankai University, Tianjin, P. R. China
Department of Mathematics, University of South Carolina, Columbia, SC 29208, USA
Beijing Computational Science Research Center, Beijing, P. R. China
qwang@math.sc.edu

Jie Shen
Department of Mathematics, Purdue University, West Lafayette, IN 47906, USA
shen7@math.purdue.edu

Received 19 October 2016
Revised 3 April 2017
Accepted 14 May 2017
Published 10 August 2017
Communicated by F. Brezzi

How to develop efficient numerical schemes while preserving energy stability at the discrete level is challenging for the three-component Cahn–Hilliard phase-field model. In this paper, we develop a set of first- and second-order temporal approximation schemes based on a novel "Invariant Energy Quadratization" approach, where all nonlinear

*Corresponding authors

terms are treated semi-explicitly. Consequently, the resulting numerical schemes lead to well-posed linear systems with a linear symmetric, positive definite at each time step. We prove that the developed schemes are unconditionally energy stable and present various 2D and 3D numerical simulations to demonstrate the stability and the accuracy of the schemes.

Keywords: Second-order; phase-field; Cahn–Hilliard; three-phase; unconditional energy stability; invariant energy quadratization.

1. Introduction

The phase-field, or the diffuse-interface method, is an efficient and robust modeling as well as computational approach to study free interface problems (cf. Refs. 1, 10, 12, 20, 23, 26, 27, 28, 32, 33, 36, 58, 62, 63, 67, 69, 70, and the references therein). Its essential idea is to use one (or more) continuous phase-field variable(s) to describe different phases in the multi-component system, and represents the interfaces by thin, smooth transition layers. The constitutive equations for the phase-field variables can be derived from the energetic variational formalism, the governing system of equations is thereby well-posed and thermodynamically consistent. Consequently, one can carry out mathematical analyses to obtain the existence and uniqueness of solutions in appropriate functional spaces, and to develop energy stable numerical schemes.

For an immiscible two-phase system, the commonly used free energy for the system consists of: (i) a double-well bulk part which promotes either of the two-phases in the bulk, yielding a hydrophobic contribution to the free energy; and (ii) a conformational capillary entropic term that promotes hydrophilic property in the multi-phase material system. The competition between the hydrophilic and hydrophobic part in the free energy enforces the coexistence of two distinctive phases in the immiscible two-phase system. The corresponding binary system can be modeled either by the Allen-Cahn equation (second-order) or the Cahn–Hilliard equation (fourth-order). For both of these models, there have been many theoretical analysis, algorithm developments and numerical simulations available in the literatures (cf. Refs. 1, 6, 7, 10, 15–19, 23, 24, 26, 28–30, 33–35, 37, 38, 44, 46, 48, 49, 51, 52, 54, 55, 59–61, 65 and 73).

The generalization from the two-phase system to multi-phase systems has been studied by many researchers (cf. Refs. 2, 3, 5–7, 15, 16, 21, 22, 29–31 and 39). Specifically, for the system with three-component, the general framework is to adopt three-independent phase variables (c_1, c_2, c_3) while imposing a hyperplane link condition among the three variables $(c_1 + c_2 + c_3 = 1)$. The bulk part of the free energy is simply a summation of the double-well potentials for each phase variable.[6,7,28] Moreover, in order to ensure the boundedness (from below) of the free energy, especially for the *total spreading* case where some coefficients of the bulk energy become negative, an extra sixth-order polynomial term is needed,[6,7] which couples the three-phase variables altogether.

Numerically, it is challenging to develop efficient schemes while preserving the energy stability to solve the three-component Cahn–Hilliard phase-field system, since all three-phase variables are nonlinearly coupled. Although a variety of numerical algorithms have been developed for it, most of the existing methods are either first-order accurate in time, or energy unstable, or highly nonlinear, or even the combinations of the above. We refer to Ref. 7 for a summary on recent advances about the three-phase models and their numerical approximations. For the development of numerical methods, we emphasize that the preservation of energy stability laws is critical to capture the correct long-time dynamics of the system especially for the preassigned grid size and time step. Furthermore, the energy-law preserving schemes provide flexibility for dealing with stiffness issue in phase-field models.

For the binary phase-field model, it is well known that the simple fully implicit or explicit scheme will induce quite severe stability conditions on the time step so that they are not efficient in practice (cf. Refs. 18, 19, 44, 45 and 53). Such phenomena appear in the computation of the three-component Cahn–Hilliard model as well (cf. the numerical examples in Ref. 7). In particular, the authors of Ref. 7 concluded that: (i) the fully implicit discretization of the sixth-order polynomial term leads to convergence of the Newton linearization method only under very tiny time step practically; (ii) it is an open problem about how to prove the existence and convergence of the numerical solution for the fully implicit scheme theoretically for the total spreading case; (iii) it is questionable to establish convex–concave decomposition for the sixth-order polynomial term; and (iv) the semi-implicit scheme is the best choice that the authors in Ref. 7 can obtain since it is unconditionally energy stable for arbitrary time step, and the existence and the convergence can be thereby proved. However, the semi-implicit schemes referred in Ref. 7 are nonlinear, thus they require some efficient iterative solvers in the implementations.

The aim of this paper is to develop stable (unconditional energy stability) and more efficient (linear) schemes to solve the three-component Cahn–Hilliard system. Instead of using traditional discretization approaches like simple implicit, stabilized explicit, convex splitting, or other various tricky Taylor expansions to discretize the nonlinear potentials, we adopt the *Invariant Energy Quadratization* (IEQ) approach that has been successfully applied in the context of other models in the authors' other work (cf. Refs. 11, 24, 55, 59–61, 64, 72 and 73). However, the application of IEQ method to the three-component Cahn–Hilliard model faces new challenges due to the particular nonlinearities including the Lagrange multiplier term, and the sixth-order polynomial potential. The essential idea of the IEQ method is to transform the free energy into a quadratic form of a new variable via a change of variables since the nonlinear potential is usually bounded from below. The new, equivalent system still retains a similar energy dissipation law in terms of new variables. For the time-continuous case, the energy law of the new reformulated system is equivalent to the energy law of the original system. A great advantage of such a reformulation is that all nonlinear terms can be treated semi-explicitly,

which in turn leads to a linear system. Moreover, the resulting linear system is symmetric positive definite, thus it can be solved efficiently with simple iterative methods such as CG or other Krylov subspace methods. Using this new strategy, we develop a series of linear and energy stable numerical schemes, without introducing artificial stabilizers as in Refs. 44, 53, 65 and 68 or using convex splitting approach (cf. Refs. 9, 17, 51 and 52).

In summary, the new numerical schemes that we develop in this paper possess the following properties: (i) the schemes are *accurate* (first- and second-order in time); (ii) they are *unconditionally energy stable*; and (iii) they are *efficient and easy to implement* (leading to symmetric positive definite linear system at each time step). To the best of our knowledge, the proposed schemes are the first such schemes for solving the three-phase Cahn–Hilliard system that can have all these desired properties. In addition, when the model is coupled with hydrodynamics (Navier–Stokes), the proposed linearization strategies can be readily applied without any essential difficulties.

The rest of the paper is organized as follows. In Sec. 2, we give a brief introduction of the three-component Cahn–Hilliard model. In Sec. 3, we construct numerical schemes and prove their unconditional energy stability and symmetric positivity for unique solvability in the time discrete case. In Sec. 4, we present various 2D and 3D numerical simulations to validate the accuracy and efficiency of the proposed schemes. Finally, some concluding remarks are presented in Sec. 5.

2. Model System

We now give a brief introduction for the three-component Cahn–Hilliard phase-field model proposed in Refs. 6 and 7. Let Ω be a smooth, open, bounded, connected domain in $\mathbb{R}^d$, $d = 2, 3$. Let c_i $(i = 1, 2, 3)$ be the ith phase-field variable which represents the volume fraction of the ith component in the fluid mixture, i.e.

$$c_i = \begin{cases} 1 & \text{inside the } i\text{th component,} \\ 0 & \text{outside the } i\text{th component.} \end{cases} \tag{2.1}$$

In the phase-field framework, a thin (of thickness ϵ) but smooth layer is used to connect the interface that is between 0 and 1. The three unknowns c_1, c_2, c_3 are linked though the constraint

$$c_1 + c_2 + c_3 = 1. \tag{2.2}$$

This is the link condition for the vector $\mathbf{C} = (c_1, c_2, c_3)$, where it belongs to the hyperplane of

$$S = \{\mathbf{C} = (c_1, c_2, c_3) \in \mathbb{R}^3, c_1 + c_2 + c_3 = 1\}. \tag{2.3}$$

In the two-phase model, the free energy of the mixture is as follows,

$$E^{\text{diph}}(c) = \int_\Omega \left(\frac{3}{4}\sigma\epsilon|\nabla c|^2 + 12\frac{\sigma}{\epsilon}c^2(1-c)^2 \right) d\mathbf{x}, \tag{2.4}$$

where σ is the surface tension parameter, the first term contributes to the hydrophilic type (tendency of mixing) of interactions between the materials and the second part, the double-well bulk energy term represents the hydrophobic type (tendency of separation) of interactions. As the consequence of the competition between the two types of interactions, the equilibrium configuration will include a diffuse interface with thickness proportional to parameter ϵ; and, as ϵ approaches zero, we expect to recover the sharp interface separating the two different materials (cf. for instance, Refs. 8, 14 and 66).

There exist several generalizations from the two-phase model to the three-phase model (cf. Refs. 6, 7 and 30). In this paper, we adopt the approach used in Ref. 7, where the free energy is defined as follows:

$$E^{\text{triph}}(c_1, c_2, c_3) = \int_\Omega \left(\frac{3}{8} \sum_{i=1}^{3} \Sigma_i \epsilon |\nabla c_i|^2 + \frac{12}{\epsilon} F(c_1, c_2, c_3) \right) d\mathbf{x}, \tag{2.5}$$

where the coefficient of entropic terms Σ_i can be negative for some specific situations.

To be algebraically consistent with the two-phase system, the three-surface tension parameters $\sigma_{12}, \sigma_{13}, \sigma_{23}$ should satisfy the following conditions:

$$\Sigma_i = \sigma_{ij} + \sigma_{ik} - \sigma_{jk}, \quad i = 1, 2, 3. \tag{2.6}$$

The nonlinear potential $F(c_1, c_2, c_3)$ is:

$$\begin{aligned} F = {} & \sigma_{12} c_1^2 c_2^2 + \sigma_{13} c_1^2 c_3^2 + \sigma_{23} c_2^2 c_3^2 + c_1 c_2 c_3 (\Sigma_1 c_1 + \Sigma_2 c_2 + \Sigma_3 c_3) \\ & + 3\Lambda c_1^2 c_2^2 c_3^2. \end{aligned} \tag{2.7}$$

Since c_1, c_2, c_3 satisfy the hyperplane link condition (2.2), the free energy can be rewritten as

$$F(c_1, c_2, c_3) = F_0(c_1, c_2, c_3) + P(c_1, c_2, c_3), \tag{2.8}$$

where

$$\begin{aligned} F_0(c_1, c_2, c_3) &= \frac{\Sigma_1}{2} c_1^2 (1 - c_1)^2 + \frac{\Sigma_2}{2} c_2^2 (1 - c_2)^2 + \frac{\Sigma_3}{2} c_3^2 (1 - c_3)^2, \\ P(c_1, c_2, c_3) &= 3\Lambda c_1^2 c_2^2 c_3^2, \end{aligned} \tag{2.9}$$

and Λ is a non-negative constant.

Here we denote ∂_i as ∂_{c_i}. We also denote by $(f(\mathbf{x}), g(\mathbf{x})) = \int_\Omega f(\mathbf{x}) g(\mathbf{x}) d\mathbf{x}$ the L^2-inner product of any two functions $f(\mathbf{x})$ and $g(\mathbf{x})$, and by $\|f\| = \sqrt{(f, f)}$ the L^2-norm of the function $f(\mathbf{x})$. We assume that the time evolution of c_i is governed by the gradient of the energy E^{triph} with respect to the $H^{-1}(\Omega)$ gradient flow, namely, the Cahn–Hilliard dynamics as follows:

$$c_{it} = \frac{M_0}{\Sigma_i} \Delta \mu_i, \tag{2.10}$$

$$\mu_i = -\frac{3}{4} \epsilon \Sigma_i \Delta c_i + \frac{12}{\epsilon} \partial_i F + \beta_L, \quad i = 1, 2, 3, \tag{2.11}$$

with the initial condition

$$c_i|_{(t=0)} = c_i^0, \quad i = 1, 2, 3, \quad c_1^0 + c_2^0 + c_3^0 = 1, \tag{2.12}$$

where β_L is the Lagrange multiplier to ensure the hyperplane link condition (2.2), that can be derived as

$$\beta_L = -\frac{4\Sigma_T}{\epsilon}\left(\frac{1}{\Sigma_1}\partial_1 F + \frac{1}{\Sigma_2}\partial_2 F + \frac{1}{\Sigma_3}\partial_3 F\right), \tag{2.13}$$

with

$$\frac{3}{\Sigma_T} = \frac{1}{\Sigma_1} + \frac{1}{\Sigma_2} + \frac{1}{\Sigma_3}. \tag{2.14}$$

We consider in this paper either of the two type boundary conditions below:

$$\text{(i)} \quad \text{all variables are periodic,} \tag{2.15}$$

$$\text{or} \quad \text{(ii)} \quad \partial_{\mathbf{n}} c_i|_{\partial\Omega} = \nabla\mu_i \cdot \mathbf{n}|_{\partial\Omega} = 0, \quad i = 1, 2, 3, \tag{2.16}$$

where $\mathbf{n}$ is the unit outward normal of the boundary $\partial\Omega$.

It is easily seen that the three chemical potentials (μ_1, μ_2, μ_3) are linked through the relation

$$\frac{\mu_1}{\Sigma_1} + \frac{\mu_2}{\Sigma_2} + \frac{\mu_3}{\Sigma_3} = 0. \tag{2.17}$$

Remark 2.1. In the physical literature, the coefficient Σ_i is called the spreading coefficient of phase i at the interface between phases j and k. Since Σ_i is determined by the surface tensions $\sigma_{i,j}$, it might not be always positive. If $\Sigma_i > 0$, the spreading is said to be "partial", and if $\Sigma_i < 0$, it is called "total".

The following lemmas hold (cf. Ref. 6):

Lemma 2.1. *There exists a constant* $\underline{\Sigma} > 0$ *such that*:

$$\Sigma_1|\xi_1|^2 + \Sigma_2|\xi_2|^2 + \Sigma_3|\xi_3|^2 \geq \underline{\Sigma}(|\xi_1|^2 + |\xi_2|^2 + |\xi_3|^2), \quad \forall\, \xi_1 + \xi_2 + \xi_3 = 0, \tag{2.18}$$

if and only if the following condition holds:

$$\Sigma_1\Sigma_2 + \Sigma_1\Sigma_3 + \Sigma_2\Sigma_3 > 0, \quad \Sigma_i + \Sigma_j > 0, \quad \forall\, i \neq j. \tag{2.19}$$

Lemma 2.2. *Let* σ_{12}, σ_{13} *and* σ_{23} *be three positive numbers and* Σ_1, Σ_2 *and* Σ_3 *defined in* (2.6). *For any* $\Lambda > 0$, *the bulk free energy* $F(c_1, c_2, c_3)$ *defined in* (2.8) *is bounded below if* c_1, c_2, c_3 *is on the hyperplane* S *in* 2D. *Furthermore, the lower bound only depends on* $\Sigma_1, \Sigma_2, \Sigma_3$ *and* Λ.

Remark 2.2. From Lemma 2.1, when (2.19) holds, the summation of the gradient entropy term is bounded below since $\nabla(c_1 + c_2 + c_3) = 0$, i.e.

$$\Sigma_1\|\nabla c_1\|^2 + \Sigma_2\|\nabla c_2\|^2 + \Sigma_3\|\nabla c_3\|^2 \geq \underline{\Sigma}(\|\nabla c_1\|^2 + \|\nabla c_2\|^2 + \|\nabla c_3\|^2) \geq 0. \tag{2.20}$$

Remark 2.3. The bulk energy $F(c_1, c_2, c_3)$ defined in (2.8) has to be bounded below in order to form a meaningful physical system. For partial spreading case

$(\Sigma_i > 0\,\forall\, i)$, one can drop the sixth-order polynomial term by assuming $\Lambda = 0$ since $F_0(c_1, c_2, c_3) \geq 0$ is naturally satisfied. For the total spreading case, Λ has to be nonzero. Moreover, to ensure the non-negativity for F, Λ has to be large enough.

For 3D case, it is shown in Ref. 6 that the bulk energy F is bounded below when $P(c_1, c_2, c_3)$ takes the following form:

$$P(c_1, c_2, c_3) = 3\Lambda c_1^2 c_2^2 c_3^2 (\phi_\alpha(c_1) + \phi_\alpha(c_2) + \phi_\alpha(c_3)), \tag{2.21}$$

where $\phi_\alpha(x) = \frac{1}{(1+x^2)^\alpha}$ with $0 < \alpha \leq \frac{8}{17}$.

Since (2.9) is commonly used in the literature (cf. Refs. 6 and 7), we adopt it here for convenience. Nonetheless, it will be clear that the numerical schemes we develop in this paper can deal with either (2.9) or (2.21) without any difficulties.

Remark 2.4. System (2.10)–(2.11) is equivalent to the following system with two-order parameters,

$$\begin{cases} c_{it} = \dfrac{M_0}{\Sigma_i}\Delta\mu_i, \\ \mu_i = -\dfrac{3}{4}\epsilon\Sigma_i\Delta c_i + \dfrac{12}{\epsilon}\partial_i F + \beta_L, \quad i = 1, 2, \\ c_3 = 1 - c_1 - c_2, \\ \dfrac{\mu_3}{\Sigma_3} = -\left(\dfrac{\mu_1}{\Sigma_1} + \dfrac{\mu_2}{\Sigma_2}\right). \end{cases} \tag{2.22}$$

We omit the detailed proof since it is quite similar to Theorem 3.1 in Sec. 3.

The model equation (2.10)–(2.11) obeys an energy dissipation law. More precisely, by taking the L^2-inner product of (2.10) with $-\mu_i$, and of (2.11) with c_{it}, and performing integration by parts, we obtain:

$$-(c_{it}, \mu_i) = \frac{M_0}{\Sigma_i}\|\nabla\mu_i\|^2, \tag{2.23}$$

$$(\mu_i, c_{it}) = \frac{3}{4}\epsilon\Sigma_i(\nabla c_i, \partial_t\nabla c_i) + \frac{12}{\epsilon}(\partial_i F, c_{it}) + (\beta_L, c_{it}). \tag{2.24}$$

Taking the summation of the two equalities for $i = 1, 2, 3$, and noticing that $(\beta_L, (c_1 + c_2 + c_3)_t) = (\beta_L, (1)_t) = 0$, we obtain the energy dissipative law:

$$\frac{d}{dt}E^{\text{triph}}(c_1, c_2, c_3) = -M_0\left(\frac{1}{\Sigma_1}\|\nabla\mu_1\|^2 + \frac{1}{\Sigma_2}\|\nabla\mu_2\|^2 + \frac{1}{\Sigma_3}\|\nabla\mu_3\|^2\right). \tag{2.25}$$

Since (μ_1, μ_2, μ_3) satisfies condition (2.17), if (2.19) holds, we have

$$-M_0\sum_{i=1}^{3}\frac{1}{\Sigma_i}\|\nabla\mu_i\|^2 \leq -M_0\underline{\Sigma}\sum_{i=1}^{3}\frac{\|\nabla\mu_i\|^2}{\Sigma_i^2} \leq 0. \tag{2.26}$$

In other words, the energy $E^{\text{triph}}(c_1, c_2, c_3)$ decays and the decay rate is $-M_0(\frac{1}{\Sigma_1}\|\nabla\mu_1\|^2 + \frac{1}{\Sigma_2}\|\nabla\mu_2\|^2 + \frac{1}{\Sigma_3}\|\nabla\mu_3\|^2)$.

3. Numerical Schemes

We develop in this section a set of linear, first- and second-order, unconditionally energy stable schemes for solving the three-component phase-field model (2.10)–(2.11). To this end, the main challenges are how to discretize the following three terms: (i) the nonlinear term associated with the double-well potential F_0; (ii) the sixth-order polynomial term P; (iii) the Lagrange multiplier term β_L, especially when some $\Sigma_i < 0$ (total spreading).

We notice that for the two-phase Cahn–Hilliard model, the discretization of the nonlinear, cubic polynomial term induced from the double-well potential had been well studied (cf. Refs. 28, 33, 35, 38 and 50). In summary, there are two commonly used techniques to discretize it in order to preserve the unconditional energy stability. The first is the convex splitting approach,[17,24,25,41,74,75] where the convex part of the potential is treated implicitly and the concave part is treated explicitly. The convex splitting approach is energy stable, however, it produces nonlinear schemes, thus the implementations are often complicated with potentially high computational costs.

The second technique is the stabilization approach[10,34,37,42–44,46–49,53,54,56,57,65,68,71] where the nonlinear term is treated explicitly. In order to preserve the energy law, a linear stabilizing term has to be added, and the magnitude of that term usually depends on the upper bound of the second-order derivative of the Ginzburg–Landau double-well potential. The stabilizer approach leads purely to linear schemes, thus it is easy to implement and solve. However, it appears that second-order schemes based on the stabilization are only conditionally energy stability.[44] On the other hand, the nonlinear potential may not satisfy the condition required for the stabilization (the generalized maximum principle). A feasible remedy is to make some reasonable revisions to the nonlinear potential outside the physically accessible regions in order to obtain a finite bound, for example, the quadratic order cut-off functions for the double-well potential (cf. Refs. 44 and 53). Such method is particularly reliable for those models with the maximum principle. However, if the maximum principle does not hold, modified nonlinear potentials may lead to spurious solutions.

For the three-component Cahn–Hilliard model system, the above two approaches cannot be easily applied. First of all, even though the convex–concave decomposition can be applied to F_0, it is not clear how to deal with the sixth-order polynomial term.[7] Second, it is uncertain whether the solution of the system satisfies a certain maximum principle so the condition required for stabilization is not satisfied. Third, unconditionally energy stable schemes are hardly obtained for both approaches if second-order schemes are considered.

We aim to develop numerical schemes that are efficient (linear system), stable (unconditionally energy stable), and accurate (up to second-order in time). To this end, we use the IEQ approach, without worrying about whether the continuous/discrete maximum principle holds or a convexity/concavity splitting exists.

3.1. *Transformed system*

Since $F(c_1, c_2, c_3)$ is always bounded below from Lemma 2.2 for 2D and Remark 2.3 for 3D, we can rewrite the free energy functional $F(c_1, c_2, c_3)$ in the following equivalent form

$$F(c_1, c_2, c_3) = (F(c_1, c_2, c_3) + B) - B, \tag{3.1}$$

where B is a constant to ensure $F(c_1, c_2, c_3) + B > 0$. In addition, we define an auxiliary function as follows,

$$U = \sqrt{F(c_1, c_2, c_3) + B}. \tag{3.2}$$

Then, the total free energy (2.5) can be rewritten as

$$E^{\text{triph}}(c_1, c_2, c_3, U) = \int_\Omega \left(\sum_{i=1}^{3} \frac{3}{8} \Sigma_i \epsilon |\nabla c_i|^2 + \frac{12}{\epsilon} U^2 \right) d\mathbf{x} - \frac{12}{\epsilon} B|\Omega|. \tag{3.3}$$

Thus, we can rewrite system (2.10)–(2.11) to the following equivalent form with four unknowns (c_1, c_2, c_3, U):

$$c_{it} = \frac{M_0}{\Sigma_i} \Delta \mu_i, \tag{3.4}$$

$$\mu_i = -\frac{3}{4} \epsilon \Sigma_i \Delta c_i + \frac{24}{\epsilon} H_i(c_1, c_2, c_3) U + \beta(c_1, c_2, c_3, U), \quad i = 1, 2, 3, \tag{3.5}$$

$$U_t = H_1(c_1, c_2, c_3) c_{1t} + H_2(c_1, c_2, c_3) c_{2t} + H_3(c_1, c_2, c_3) c_{3t}, \tag{3.6}$$

where

$$\begin{cases} H_1(c_1, c_2, c_3) = \dfrac{\delta U}{\delta c_1} = \dfrac{1}{2} \dfrac{\frac{\Sigma_1}{2}(c_1 - c_1^2)(1 - 2c_1) + 6\Lambda c_1 c_2^2 c_3^2}{\sqrt{F(c_1, c_2, c_3) + B}}, \\ H_2(c_1, c_2, c_3) = \dfrac{\delta U}{\delta c_2} = \dfrac{1}{2} \dfrac{\frac{\Sigma_2}{2}(c_2 - c_2^2)(1 - 2c_2) + 6\Lambda c_1^2 c_2 c_3^2}{\sqrt{F(c_1, c_2, c_3) + B}}, \\ H_3(c_1, c_2, c_3) = \dfrac{\delta U}{\delta c_3} = \dfrac{1}{2} \dfrac{\frac{\Sigma_3}{2}(c_3 - c_3^2)(1 - 2c_3) + 6\Lambda c_1^2 c_2^2 c_3}{\sqrt{F(c_1, c_2, c_3) + B}}, \\ \beta(c_1, c_2, c_3, U) = -\dfrac{8}{\epsilon} \Sigma_T U \displaystyle\sum_{i=1}^{3} \frac{1}{\Sigma_i} H_i(c_1, c_2, c_3). \end{cases} \tag{3.7}$$

The transformed system (3.4)–(3.6) in the variables (c_1, c_2, c_3, U) form a closed PDE system with the following initial conditions,

$$\begin{cases} c_i(t = 0) = c_i^0, \quad i = 1, 2, 3, \\ U(t = 0) = U^0 = \sqrt{F(c_1^0, c_2^0, c_3^0) + B}. \end{cases} \tag{3.8}$$

Note that we do not need any boundary conditions for U since Eq. (3.6) for it is only ordinary differential equation with respect to time, i.e. the boundary conditions of the new system (3.4)–(3.6) are still (2.16).

Remark 3.1. The system (3.4)–(3.6) is equivalent to the following two-order parameter system

$$\begin{cases} c_{it} = \dfrac{M_0}{\Sigma_i}\Delta\mu_i, \\ \mu_i = -\dfrac{3}{4}\epsilon\Sigma_i\Delta c_i + \dfrac{24}{\epsilon}H_iU + \beta, \quad i = 1, 2, \\ U_t = H_1c_{1t} + H_2c_{2t} + H_3c_{3t}, \end{cases} \tag{3.9}$$

with

$$\begin{aligned} c_3 &= 1 - c_1 - c_2, \\ \frac{\mu_3}{\Sigma_3} &= -\left(\frac{\mu_1}{\Sigma_1} + \frac{\mu_2}{\Sigma_2}\right). \end{aligned} \tag{3.10}$$

Since the proof is quite similar to Theorem 3.1, we omit the details here.

We can easily obtain the energy law for the new system (3.4)–(3.6). Taking the L^2-inner product of (3.4) with $-\mu_i$, of (3.5) with $\partial_t c_i$, of (3.6) with $-\frac{24}{\epsilon}U$, taking the summation for $i = 1, 2, 3$, and noticing that $(\beta, \partial_t(c_1 + c_2 + c_3)) = 0$ from Remark 3.1, we obtain the energy dissipation law as follows:

$$\begin{aligned} \frac{d}{dt}E^{\text{triph}}(c_1, c_2, c_3, U) &= -M_0\left(\frac{1}{\Sigma_1}\|\nabla\mu_1\|^2 + \frac{1}{\Sigma_2}\|\nabla\mu_2\|^2 + \frac{1}{\Sigma_3}\|\nabla\mu_3\|^2\right) \\ &\le -M_0\underline{\Sigma}\left(\frac{\|\nabla\mu_1\|^2}{\Sigma_1^2} + \frac{\|\nabla\mu_2\|^2}{\Sigma_2^2} + \frac{\|\nabla\mu_3\|^2}{\Sigma_3^2}\right) \le 0. \end{aligned} \tag{3.11}$$

Remark 3.2. The new transformed system (3.4)–(3.6) is equivalent to the original system (2.10)–(2.11) since (3.2) can be obtained by integrating (3.6) with respect to time. Therefore, the energy law (3.11) for the transformed system is exactly the same as the energy law (2.25) for the original system. We emphasize that we will develop energy stable numerical schemes for the new transformed system (3.4)–(3.6). The proposed schemes will follow a discrete energy law corresponding to (3.11) instead of the energy law for the original system (2.25).

3.2. *First-order scheme*

We now present the first-order time stepping scheme to solve the system (3.4)–(3.6) where the time derivative is discretized based on the first-order backward Euler method.

We fix the notations here. Let $\delta t > 0$ denote the time step size and set $t^n = n\,\delta t$ for $0 \le n \le N$ with $T = N\delta t$.

Assuming that $(c_1, c_2, c_3, U)^n$ are already calculated, we compute $(c_1, c_2, c_3, U)^{n+1}$ from the following temporal discrete system:

$$\frac{c_i^{n+1} - c_i^n}{\delta t} = \frac{M_0}{\Sigma_i}\Delta\mu_i^{n+1}, \tag{3.12}$$

$$\mu_i^{n+1} = -\frac{3}{4}\epsilon\Sigma_i\Delta c_i^{n+1} + \frac{24}{\epsilon}H_i^n U^{n+1} + \beta^{n+1}, \quad i = 1, 2, 3, \tag{3.13}$$

$$U^{n+1} - U^n = H_1^n(c_1^{n+1} - c_1^n) + H_2^n(c_2^{n+1} - c_2^n) + H_3^n(c_3^{n+1} - c_3^n), \tag{3.14}$$

where

$$\begin{cases} H_1^n = \dfrac{1}{2}\dfrac{\frac{\Sigma_1}{2}(c_1^n - {c_1^n}^2)(1 - 2c_1^n) + 6\Lambda c_1^n {c_2^n}^2 {c_3^n}^2}{\sqrt{F(c_1^n, c_2^n, c_3^n) + B}}, \\ H_2^n = \dfrac{1}{2}\dfrac{\frac{\Sigma_2}{2}(c_2^n - {c_2^n}^2)(1 - 2c_2^n) + 6\Lambda {c_1^n}^2 c_2^n {c_3^n}^2}{\sqrt{F(c_1^n, c_2^n, c_3^n) + B}}, \\ H_3^n = \dfrac{1}{2}\dfrac{\frac{\Sigma_3}{2}(c_3^n - {c_3^n}^2)(1 - 2c_3^n) + 6\Lambda {c_1^n}^2 {c_2^n}^2 c_3^n}{\sqrt{F(c_1^n, c_2^n, c_3^n) + B}}, \\ \beta^{n+1} = -\dfrac{8}{\epsilon}\Sigma_T\left(\dfrac{1}{\Sigma_1}H_1^n + \dfrac{1}{\Sigma_2}H_2^n + \dfrac{1}{\Sigma_3}H_3^n\right)U^{n+1}. \end{cases} \tag{3.15}$$

The initial conditions are (3.8), and the boundary conditions are:

$$\text{(i) all variables are periodic;} \quad \text{or} \quad \text{(ii) } \partial_{\mathbf{n}} c_i^{n+1}|_{\partial\Omega} = \nabla\mu_i^{n+1}\cdot\mathbf{n}|_{\partial\Omega} = 0, \quad i = 1, 2, 3. \tag{3.16}$$

We immediately derive the following result which ensures the numerical solutions satisfy the hyperplane condition (2.2).

Theorem 3.1. *System of* (3.12)–(3.14) *is equivalent to the following scheme with two-order parameters*:

$$\frac{c_i^{n+1} - c_i^n}{\delta t} = \frac{M_0}{\Sigma_i}\Delta\mu_i^{n+1}, \tag{3.17}$$

$$\mu_i^{n+1} = -\frac{3}{4}\epsilon\Sigma_1\Delta c_i^{n+1} + \frac{24}{\epsilon}H_i^n U^{n+1} + \beta^{n+1}, \quad i = 1, 2, \tag{3.18}$$

$$U^{n+1} - U^n = H_1^n(c_1^{n+1} - c_1^n) + H_2^n(c_2^{n+1} - c_2^n) + H_3^n(c_3^{n+1} - c_3^n), \tag{3.19}$$

with

$$c_3^{n+1} = 1 - c_1^{n+1} - c_2^{n+1}, \tag{3.20}$$

$$\frac{\mu_3^{n+1}}{\Sigma_3} = -\left(\frac{\mu_1^{n+1}}{\Sigma_1} + \frac{\mu_2^{n+1}}{\Sigma_2}\right). \tag{3.21}$$

Proof. From (3.15), we can easily show that the following identity holds,

$$\frac{24}{\epsilon}\left(\frac{H_1^n}{\Sigma_1} + \frac{H_2^n}{\Sigma_2} + \frac{H_3^n}{\Sigma_3}\right)U^{n+1} + \beta^{n+1}\left(\frac{1}{\Sigma_1} + \frac{1}{\Sigma_2} + \frac{1}{\Sigma_3}\right) = 0. \tag{3.22}$$

- We first assume that (3.17)–(3.21) are satisfied, and derive (3.12)–(3.13). By taking the summation of (3.17) for $i = 1, 2$, and applying (3.20) and (3.21), we obtain

$$\frac{c_3^{n+1} - c_3^n}{\delta t} = \frac{M_0}{\Sigma_3} \Delta \mu_3^{n+1}. \tag{3.23}$$

From (3.18), (3.20)–(3.22), we obtain

$$\begin{aligned} \mu_3^{n+1} &= -\Sigma_3 \left(\frac{\mu_1^{n+1}}{\Sigma_1} + \frac{\mu_2^{n+1}}{\Sigma_2} \right) \\ &= -\Sigma_3 \left(-\frac{3}{4}\epsilon \Delta c_1^{n+1} - \frac{3}{4}\epsilon \Delta c_2^{n+1} + \frac{24}{\epsilon} \left(\frac{H_1^n}{\Sigma_1} + \frac{H_2^n}{\Sigma_2} \right) U^{n+1} \right. \\ &\quad \left. + \beta^{n+1} \left(\frac{1}{\Sigma_1} + \frac{1}{\Sigma_2} \right) \right) \\ &= \frac{3}{4}\epsilon \Sigma_3 \Delta c_3^{n+1} + \frac{24}{\epsilon} H_3^n U^{n+1} + \beta^{n+1}. \end{aligned} \tag{3.24}$$

- We then assume that (3.12)–(3.13) are satisfied and derive (3.17)–(3.21). By taking the summation of (3.12) for $i = 1, 2, 3$, we derive

$$\frac{S^{n+1} - S^n}{\delta t} = M_0 \Delta \Theta^{n+1}, \tag{3.25}$$

where $S^n = c_1^n + c_2^n + c_3^n$ and $\Theta^{n+1} = \frac{1}{\Sigma_1}\mu_1^{n+1} + \frac{1}{\Sigma_2}\mu_2^{n+1} + \frac{1}{\Sigma_3}\mu_3^{n+1}$. From (3.13) and (3.22), we derive

$$\Theta^{n+1} = -\frac{3}{4}\epsilon \Delta S^{n+1}. \tag{3.26}$$

By taking the L^2-inner product of (3.25) with $-\Theta^{n+1}$, of (3.26) with $S^{n+1} - S^n$, and taking the summation of the two equalities above, we derive

$$\frac{3}{8}\epsilon (\|\nabla S^{n+1}\|^2 - \|\nabla S^n\|^2 + \|\nabla S^{n+1} - \nabla S^n\|^2) + \delta t M_0 \|\nabla \Theta^{n+1}\|^2 = 0. \tag{3.27}$$

Since $S^n = 1$, the left-hand side of (3.27) is a sum of non-negative terms, thus $\nabla S^{n+1} = 0$, and $\nabla \Theta^{n+1} = 0$, i.e. the functions S^{n+1} and Θ^{n+1} are constants. Then (3.26) leads to $\Theta^{n+1} = 0$, and (3.25) leads to $S^{n+1} = S^n = 1$. Thus, we obtain (3.20). By dividing Σ_i for (3.13) and taking the summation of it for $i = 1, 2, 3$, and applying (3.22) and (3.20), we obtain (3.21). □

The most interesting property of the above scheme is that the nonlinear coefficient H_i of the new variable U are treated explicitly, which can tremendously speed up the computation in practice. More specifically, we can rewrite Eq. (3.14) as follows:

$$U^{n+1} = H_1^n c_1^{n+1} + H_2^n c_2^{n+1} + H_3^n c_3^{n+1} + Q_1^n, \tag{3.28}$$

where $Q_1^n = U^n - H_1^n c_1^n - H_2^n c_2^n - H_3^n c_3^n$. Thus, the system (3.12)–(3.14) can be rewritten as:

$$\frac{c_i^{n+1} - c_i^n}{\delta t} = \frac{M_0}{\Sigma_i} \Delta \mu_i^{n+1}, \tag{3.29}$$

$$\mu_i^{n+1} = -\frac{3}{4}\epsilon \Sigma_i \Delta c_i^{n+1} + \frac{24}{\epsilon} H_i^n (H_1^n c_1^{n+1} + H_2^n c_2^{n+1} + H_3^n c_3^{n+1}) + \overline{\beta}^{n+1} + g_i^n, \quad i = 1, 2, 3, \tag{3.30}$$

where

$$\begin{cases} \overline{\beta}^{n+1} = -\dfrac{8}{\epsilon} \Sigma_T \left(\dfrac{1}{\Sigma_1} H_1^n + \dfrac{1}{\Sigma_2} H_2^n + \dfrac{1}{\Sigma_3} H_3^n \right) (H_1^n c_1^{n+1} + H_2^n c_2^{n+1} + H_3^n c_3^{n+1}), \\ g_i^n = \dfrac{24}{\epsilon} H_i^n Q_1^n - \dfrac{8}{\epsilon} \Sigma_T \left(\dfrac{1}{\Sigma_1} H_1^n + \dfrac{1}{\Sigma_2} H_2^n + \dfrac{1}{\Sigma_3} H_3^n \right) Q_1^n. \end{cases}$$

Theorem 3.2. *Assuming* (2.19), *linear system* (3.29)–(3.30) *for the variable* $\mathbf{C} = (c_1^{n+1}, c_2^{n+1}, c_3^{n+1})^T$ *is symmetric* (*self-adjoint*) *and positive definite.*

Proof. Taking the L^2-inner product of (3.29) with 1, we derive

$$\int_\Omega c_i^{n+1} d\mathbf{x} = \int_\Omega c_i^n d\mathbf{x} = \cdots = \int_\Omega c_i^0 d\mathbf{x}. \tag{3.31}$$

Let $\alpha_i^0 = \frac{1}{|\Omega|} \int_\Omega c_i^0 d\mathbf{x}$, $\gamma_i^0 = \frac{1}{|\Omega|} \int_\Omega \mu_i^{n+1} d\mathbf{x}$, and define

$$\widehat{c}_i^{\,n+1} = c_i^{n+1} - \alpha_i^0, \quad \widehat{\mu}_i^{\,n+1} = \mu_i^{n+1} - \gamma_i^0. \tag{3.32}$$

Thus, from (3.29)–(3.30), $(\widehat{c}_i^{\,n+1}, \widehat{\mu}_i^{\,n+1})$ are the solutions for the following equations with unknowns (C_i, μ_i),

$$\frac{C_i}{M_0 \delta t} - \frac{1}{\Sigma_i} \Delta \mu_i = \frac{\widehat{c}_i^{\,n}}{M_0 \delta t}, \tag{3.33}$$

$$\mu_i + \gamma_i^0 = -\frac{3}{4}\epsilon \Sigma_i \Delta C_i + \frac{24}{\epsilon} H_i^n P(C_1, C_2, C_3) + \widehat{\beta}(C_1, C_2, C_3) + \widehat{g}_i^{\,n}, \tag{3.34}$$

where

$$\begin{cases} P(C_1, C_2, C_3) = H_1^n C_1 + H_2^n C_2 + H_3^n C_3, \\ \widehat{\beta}(C_1, C_2, C_3) = -\dfrac{8}{\epsilon} \Sigma_T \left(\dfrac{1}{\Sigma_1} H_1^n + \dfrac{1}{\Sigma_2} H_2^n + \dfrac{1}{\Sigma_3} H_3^n \right) P(C_1, C_2, C_3), \end{cases}$$

and g_i^n includes all known terms in the nth step, and

$$C_1 + C_2 + C_3 = 0, \quad \int_\Omega C_i d\mathbf{x} = 0, \quad \int_\Omega \mu_i d\mathbf{x} = 0. \tag{3.35}$$

We define the inverse Laplace operator u (with $\int_\Omega u d\mathbf{x} = 0$) $\mapsto v := \Delta^{-1} u$ by

$$\begin{cases} \Delta v = u, \quad \int_\Omega v d\mathbf{x} = 0, \\ \quad \text{with the boundary conditions either (i) } v \text{ is periodic; or (ii) } \partial_{\mathbf{n}} v|_{\partial\Omega} = 0. \end{cases} \tag{3.36}$$

Applying $-\Delta^{-1}$ to (3.33) and using (3.34), we obtain

$$\begin{aligned} &-\frac{\Sigma_i}{M_0 \delta t} \Delta^{-1} C_i - \frac{3}{4} \epsilon \Sigma_i \Delta C_i + \frac{24}{\epsilon} H_i^n P(C_1, C_2, C_3) + \widehat{\beta}(C_1, C_2, C_3) - \gamma_i^0 \\ &\quad = -\Sigma_i \Delta^{-1} \frac{\widehat{c}_i^n}{M_0 \delta t} - \widehat{g}_i^n, \quad i = 1, 2, 3. \end{aligned} \tag{3.37}$$

We consider the weak form of the above system, i.e. for any $i = 1, 2, 3$, $D_i \in H^1(\Omega)$ with $\int_\Omega D_i d\mathbf{x} = 0$ and $\sum_{i=1}^3 D_i = 0$, we have

$$\begin{aligned} &-\frac{\Sigma_i}{M_0 \delta t} (\Delta^{-1} C_i, D_i) + \frac{3}{4} \epsilon \Sigma_i (\nabla C_i, \nabla D_i) + \frac{24}{\epsilon} (H_i^n P, D_i) + (\widehat{\beta}, D_i) \\ &\quad = \left(-\Sigma_i \Delta^{-1} \frac{\widehat{c}_i^n}{M_0 \delta t} - \widehat{g}_i^n, D_i \right), \quad i = 1, 2, 3. \end{aligned} \tag{3.38}$$

We express the above linear system (3.38) as $(\mathbb{A}\mathbf{C}, \mathbf{D}) = (\mathbf{b}, \mathbf{D})$, where $\mathbf{C} = (C_1, C_2, C_3)^T$ and $\mathbf{D} = (D_1, D_2, D_3)^T$.

We can easily derive

$$(\mathbb{A}\mathbf{C}, \mathbf{D}) = (\mathbf{C}, \mathbb{A}\mathbf{D}), \tag{3.39}$$

thus $\mathbb{A}$ is self-adjoint.

Moreover, from $\sum_{i=1}^3 C_i = 0$, we have

$$\begin{aligned} (\mathbb{A}\mathbf{C}, \mathbf{C}) = &\frac{1}{M_0 \delta t} (\Sigma_1 (-\Delta^{-1} C_1, C_1) + \Sigma_2 (-\Delta^{-1} C_2, C_2) + \Sigma_3 (-\Delta^{-1} C_3, C_3)) \\ &+ \frac{3}{4} \epsilon \sum_{i=1}^3 \Sigma_i \|\nabla C_i\|^2 + \frac{24}{\epsilon} \|H_1^n C_1 + H_2^n C_2 + H_3^n C_3\|^2. \end{aligned} \tag{3.40}$$

Let $d_i = \Delta^{-1} C_i$, i.e.

$$\Delta d_i = C_i, \quad \int_\Omega d_i d\mathbf{x} = 0, \tag{3.41}$$

with periodic boundary conditions or $\partial_{\mathbf{n}} d_i|_{\partial\Omega} = 0$. Therefore, we have

$$(-\Delta^{-1} C_i, C_i) = \|\nabla d_i\|^2. \tag{3.42}$$

Furthermore, $Z = d_1 + d_2 + d_3$ satisfies

$$\Delta Z = 0, \quad \int_\Omega Z d\mathbf{x} = 0, \tag{3.43}$$

with periodic boundary conditions or $\partial_{\mathbf{n}} Z|_{\partial\Omega} = 0$. Thus, $Z = d_1 + d_2 + d_3 = 0$. From (2.20), we derive

$$\begin{aligned}(\mathbb{A}\mathbf{C}, \mathbf{C}) \geq & \frac{1}{M_0 \delta t} \underline{\Sigma} (\|\nabla d_1\|^2 + \|\nabla d_2\|^2 + \|\nabla d_3\|^2) \\ & + \frac{3}{4} \underline{\Sigma} \epsilon (\|\nabla C_1\|^2 + \|\nabla C_2\|^2 + \|\nabla C_3\|^2) \\ & + \frac{24}{\epsilon} \|H_1^n C_1 + H_2^n C_2 + H_3^n C_3\|^2 \geq 0, \end{aligned} \tag{3.44}$$

and $(\mathbb{A}\mathbf{C}, \mathbf{C}) = \mathbf{0}$ if and only if $\mathbf{C} = \mathbf{0}$. Thus, we conclude the theorem. □

Remark 3.3. We can show the well-posedness of the linear system $(\mathbb{A}\mathbf{C}, \mathbf{D}) = (\mathbf{b}, \mathbf{D})$ from the Lax–Milgram theorem noticing that the linear operator $\mathbb{A}$ is bounded and coercive in $H^1(\Omega)$. We leave the detailed proof to the interested readers since the proof is rather standard.

Remark 3.4. From Theorem 3.1, the linear system (3.12)–(3.14) with three unknowns and the linear system (3.17)–(3.19) with two unknowns, are equivalent. In our numerical tests, we find that the solutions of these two schemes are identical up to the machine accuracy.

In practice, we directly solve the linear system (3.29)–(3.30) instead of using the inverse Laplacian operator $(-\Delta)^{-1}$ since it is a non-local operator and thus it is not efficient to implement in physical space. Moreover, notice that the term $H_i^n(H_1^n c_1^{n+1} + H_2^n c_2^{n+1} + H_3^n c_3^{n+1})$ in (3.30) will lead to a full matrix, therefore, we use a preconditioned conjugate gradient (PCG) method with an optimal preconditioner constructed by an approximate problem of (3.30) where $H_i^n H_j^n$ is replaced by a constant $\max_{\forall \mathbf{x}}(H_i^n H_j^n)$. In this way, the system (3.29)–(3.30) can be solved very efficiently.

The stability result of the first-order scheme (3.12)–(3.14) is given below.

Theorem 3.3. *When* (2.19) *holds, the first-order linear scheme given in* (3.12)–(3.14) *is unconditionally energy stable, i.e. satisfies the following discrete energy dissipation law*:

$$\frac{1}{\delta t}(E_{1st}^{n+1} - E_{1st}^n) \leq -M_0 \underline{\Sigma} \left(\frac{\|\nabla \mu_1^{n+1}\|^2}{\Sigma_1^2} + \frac{\|\nabla \mu_2^{n+1}\|^2}{\Sigma_2^2} + \frac{\|\nabla \mu_3^{n+1}\|^2}{\Sigma_3^2} \right), \tag{3.45}$$

where E_{1st}^n *is defined by*

$$E_{1st}^n = \frac{3}{8}\Sigma_1 \epsilon \|\nabla c_1^n\|^2 + \frac{3}{8}\Sigma_2 \epsilon \|\nabla c_2^n\|^2 + \frac{3}{8}\Sigma_3 \epsilon \|\nabla c_3^n\|^2 + \frac{12}{\epsilon}\|U^n\|^2 - \frac{12}{\epsilon} B|\Omega|. \tag{3.46}$$

Proof. Taking the L^2-inner product of (3.12) with $-\delta t \mu_i^{n+1}$, we obtain

$$-(c_i^{n+1} - c_i^n, \mu_i^{n+1}) = \delta t \frac{M_0}{\Sigma_i} \|\nabla \mu_i^{n+1}\|^2. \tag{3.47}$$

Taking the L^2-inner product of (3.13) with $c_i^{n+1} - c_i^n$ and applying the following identities

$$2(a-b,a) = |a|^2 - |b|^2 + |a-b|^2, \tag{3.48}$$

we derive

$$\begin{aligned}(\mu_i^{n+1}, c_i^{n+1} - c_i^n) = \frac{3}{8}\epsilon\Sigma_i(\|\nabla c_i^{n+1}\|^2 - \|\nabla c_i^n\|^2 + \|\nabla c_i^{n+1} - \nabla c_i^n\|^2) \\ + \frac{24}{\epsilon}(H_i^n U^{n+1}, c_i^{n+1} - c_i^n) + (\beta^{n+1}, c_i^{n+1} - c_i^n).\end{aligned} \tag{3.49}$$

Taking the L^2-inner product of (3.14) with $\frac{24}{\epsilon}U^{n+1}$, we obtain

$$\begin{aligned}&\frac{12}{\epsilon}(\|U^{n+1}\|^2 - \|U^n\|^2 + \|U^{n+1} - U^n\|^2) \\ &\quad = \frac{24}{\epsilon}\Big((H_1^n(c_1^{n+1} - c_1^n), U^{n+1})(H_2^n(c_2^{n+1} - c_2^n), U^{n+1}) \\ &\qquad + (H_3^n(c_3^{n+1} - c_3^n), U^{n+1})\Big).\end{aligned} \tag{3.50}$$

Combining (3.47), (3.49), taking the summation for $i = 1, 2, 3$ and using (3.50) and (3.20), we have

$$\begin{aligned}&\frac{3}{8}\epsilon\sum_{i=1}^3 \Sigma_i(\|\nabla c_i^{n+1}\|^2 - \|\nabla c_i^n\|^2) + \frac{3}{8}\epsilon\sum_{i=1}^3 \Sigma_i\|\nabla c_i^{n+1} - \nabla c_i^n\|^2 \\ &\qquad + \frac{12}{\epsilon}(\|U^{n+1}\|^2 - \|U^n\|^2) \\ &\qquad = -M_0\left(\frac{1}{\Sigma_1}\|\nabla\mu_1^{n+1}\|^2 + \frac{1}{\Sigma_2}\|\nabla\mu_2^{n+1}\|^2 + \frac{1}{\Sigma_3}\|\nabla\mu_3^{n+1}\|^2\right) \\ &\qquad \le -M_0\underline{\Sigma}(\|\nabla\mu_1^{n+1}\|^2 + \|\nabla\mu_2^{n+1}\|^2 + \|\nabla\mu_3^{n+1}\|^2) \le 0,\end{aligned} \tag{3.51}$$

where the term associated with β^{n+1} vanishes since $\sum_{i=1}^3 c_i^{n+1} = \sum_{i=1}^3 c_i^n = 1$.

Noticing that $\sum_{i=1}^3 \nabla(c_i^{n+1} - c_i^n) = 0$, we derive

$$\sum_{i=1}^3(\Sigma_i\|\nabla c_i^{n+1} - \nabla c_i^n\|^2) \ge \underline{\Sigma}\sum_{i=1}^3(\|\nabla c_i^{n+1} - \nabla c_i^n\|^2) \ge 0. \tag{3.52}$$

Therefore, the desired result (3.45) is obtained after we drop this positive term.

□

Remark 3.5. We remark that the discrete energy E_{1st} defined in (3.46) is bounded below. Such property is particularly significant. Otherwise, energy stability does not make any sense.

The essential idea of the IEQ method is to transform the complicated nonlinear potentials into a simple quadratic form in terms of some new variables via a change

of variables. Such a simple way of quadratization provides some great advantages. First, the complicated nonlinear potential is transferred to a quadratic polynomial form that is much easier to handle. Second, the derivative of the quadratic polynomial is linear, which provides the fundamental support for linearization. Third, the quadratic formulation in terms of new variables can automatically keep the nonlinear potential bounded below. We notice that the convexity is required in the convex splitting approach[17]; and the boundedness for the second-order derivative is required in the stabilization approach.[44,53] Compared with those two methods, the IEQ method provides much more flexibilities to treat the complicated nonlinear terms since the only request of it is that the nonlinear potential is bounded below.

Meanwhile, the choice of new variables is not unique. For instance, for the partial spreading case where $\Sigma_i > 0$, $\forall\, i$, we can define four functions $\widehat{U}_1, \widehat{U}_2, \widehat{U}_3, V$ as follows:

$$\begin{aligned} \widehat{U}_i &= c_i(1-c_i), \quad i = 1,2,3, \\ V &= c_1 c_2 c_3. \end{aligned} \tag{3.53}$$

Thus, the free energy becomes

$$\begin{aligned} E(\widehat{U}_1, \widehat{U}_2, \widehat{U}_3, V) = \int_\Omega \Bigg(& \frac{3}{8}\Sigma_1 \epsilon |\nabla c_1|^2 + \frac{3}{8}\Sigma_2 \epsilon |\nabla c_2|^2 + \frac{3}{8}\Sigma_3 \epsilon |\nabla c_3|^2 \\ & + \frac{12}{\epsilon}\left(\frac{\Sigma_1}{2}\widehat{U}_1^2 + \frac{\Sigma_2}{2}\widehat{U}_2^2 + \frac{\Sigma_3}{2}\widehat{U}_3^2 + 3\Lambda V^2 \right) \Bigg) d\mathbf{x}. \end{aligned} \tag{3.54}$$

For this new definition of the free energy, one can carry out a similar analysis. The details are left to the interested readers. However, we notice that this particular transformation only works for the partial spreading case. For the total spreading case, since for some i, $\Sigma_i < 0$, the energy defined in (3.54) may not be bounded below. This is the particular reason why we define the new variable U in (3.2) in this paper.

As it is shown, the IEQ approach is able to provide enough flexibilities to derive the equivalent PDE system, which then leads to corresponding numerical schemes with desired properties such as unconditional energy stability and linearity.

Remark 3.6. The proposed scheme follows the new energy dissipation law (3.11) instead of the energy law for the originated system (2.25). For time-continuous case, (3.11) and (2.25) are identical. For time-discrete case, the discrete energy law (3.45) is the first-order approximation to the new energy law (3.11). Moreover, the discrete energy functional E_{1st}^{n+1} is also the first-order approximation to $E(\phi^{n+1})$ (defined in (2.5)), since U^{n+1} is the first-order approximations to $\sqrt{F(c_1^{n+1}, c_2^{n+1}, c_3^{n+1}) + B}$, that can be observed from the following facts, heuristically. We rewrite (3.14) as

follows:

$$U^{n+1}-\sqrt{F(c_1^{n+1},c_2^{n+1},c_3^{n+1})+B}=U^n-\sqrt{F(c_1^n,c_2^n,c_3^n)+B}+R_{n+1}, \quad (3.55)$$

where $R_{n+1}=O(\sum_{i=1}^{3}(c_i^{n+1}-c_i^n)^2)$. Since $R_k=O(\delta t^2)$ for $0\le k\le n+1$ and $U^0=\sqrt{F(c_1^0,c_2^0,c_3^0)+B}$, then by mathematical induction we can easily get

$$U^{n+1}=\sqrt{F(c_1^{n+1},c_2^{n+1},c_3^{n+1})+B}+O(\delta t). \quad (3.56)$$

3.3. *Second-order scheme based on Crank–Nicolson*

We now present a second-order time stepping scheme to solve the system (3.4)–(3.6).

Assuming that $(c_1,c_2,c_3,U)^n$ and $(c_1,c_2,c_3,U)^{n-1}$ are already calculated, we compute $(c_1,\ c_2,\ c_3,\ U)^{n+1}$ from the following temporal discrete system:

$$c_{it}=\frac{M_0}{\Sigma_i}\Delta\mu_i^{n+\frac{1}{2}}, \quad (3.57)$$

$$\mu_i^{n+\frac{1}{2}}=-\frac{3}{4}\epsilon\Sigma_i\Delta\frac{c_i^{n+1}+c_i^n}{2}+\frac{24}{\epsilon}H_i^{*,n+\frac{1}{2}}U^{n+\frac{1}{2}}+\beta^{n+\frac{1}{2}}, \quad i=1,2,3, \quad (3.58)$$

$$\begin{aligned}U^{n+1}-U^n&=H_1^{*,n+\frac{1}{2}}(c_1^{n+1}-c_1^n)+H_2^{*,n+\frac{1}{2}}(c_2^{n+1}-c_2^n)\\&\quad+H_3^{*,n+\frac{1}{2}}(c_3^{n+1}-c_3^n),\end{aligned} \quad (3.59)$$

where

$$\begin{cases}U^{n+\frac{1}{2}}=\dfrac{U^{n+1}+U^n}{2},\\[2ex] c_i^{*,n+\frac{1}{2}}=\dfrac{3}{2}c_i^n-\dfrac{1}{2}c_i^{n-1},\\[2ex] H_1^{*,n+\frac{1}{2}}=\dfrac{1}{2}\dfrac{\frac{\Sigma_1}{2}\left(c_1^{*,n+\frac{1}{2}}-\left(c_1^{*,n+\frac{1}{2}}\right)^2\right)\left(1-2c_1^{*,n+\frac{1}{2}}\right)+6\Lambda c_1^{*,n+\frac{1}{2}}\left(c_2^{*,n+\frac{1}{2}}\right)^2\left(c_3^{*,n+\frac{1}{2}}\right)^2}{\sqrt{F\left(c_1^{*,n+\frac{1}{2}},c_2^{*,n+\frac{1}{2}},c_3^{*,n+\frac{1}{2}}\right)+B}},\\[2ex] H_2^{*,n+\frac{1}{2}}=\dfrac{1}{2}\dfrac{\frac{\Sigma_2}{2}\left(c_2^{*,n+\frac{1}{2}}-\left(c_2^{*,n+\frac{1}{2}}\right)^2\right)\left(1-2c_2^{*,n+\frac{1}{2}}\right)+6\Lambda\left(c_1^{*,n+\frac{1}{2}}\right)^2c_2^{*,n+\frac{1}{2}}\left(c_3^{*,n+\frac{1}{2}}\right)^2}{\sqrt{F\left(c_1^{*,n+\frac{1}{2}},c_2^{*,n+\frac{1}{2}},c_3^{*,n+\frac{1}{2}}\right)+B}},\\[2ex] H_3^{*,n+\frac{1}{2}}=\dfrac{1}{2}\dfrac{\frac{\Sigma_3}{2}\left(c_3^{*,n+\frac{1}{2}}-\left(c_3^{*,n+\frac{1}{2}}\right)^2\right)\left(1-2c_3^{*,n+\frac{1}{2}}\right)+6\Lambda\left(c_1^{*,n+\frac{1}{2}}\right)^2\left(c_2^{*,n+\frac{1}{2}}\right)^2c_3^{*,n+\frac{1}{2}}}{\sqrt{F\left(c_1^{*,n+\frac{1}{2}},c_2^{*,n+\frac{1}{2}},c_3^{*,n+\frac{1}{2}}\right)+B}},\\[2ex] \beta^{n+\frac{1}{2}}=-\dfrac{8}{\epsilon}\Sigma_T\left(\dfrac{1}{\Sigma_1}H_1^{*,n+\frac{1}{2}}+\dfrac{1}{\Sigma_2}H_2^{*,n+\frac{1}{2}}+\dfrac{1}{\Sigma_3}H_3^{*,n+\frac{1}{2}}\right)U^{n+\frac{1}{2}}.\end{cases} \quad (3.60)$$

The initial conditions are (3.8) and the boundary conditions are:

$$\text{(i) all variables are periodic;} \quad \text{or} \quad \text{(ii) } \partial_{\mathbf{n}} c_i^{n+1}|_{\partial\Omega} = \nabla \mu_i^{n+\frac{1}{2}} \cdot \mathbf{n}|_{\partial\Omega} = 0, \quad i = 1, 2, 3. \tag{3.61}$$

The following theorem ensures that the numerical solution $(c_1^{n+1}, c_2^{n+1}, c_3^{n+1})$ always satisfies the hyperplane link condition (2.2).

Theorem 3.4. *System* (3.57)–(3.59) *is equivalent to the following scheme with two-order parameters*:

$$\frac{c_i^{n+1} - c_i^n}{\delta t} = \frac{M_0}{\Sigma_i} \Delta \mu_i^{n+\frac{1}{2}}, \tag{3.62}$$

$$\mu_i^{n+\frac{1}{2}} = -\frac{3}{4}\epsilon\Sigma_i \Delta \frac{c_i^{n+1} + c_i^n}{2} + \frac{24}{\epsilon} H_i^{*,n+\frac{1}{2}} U^{n+\frac{1}{2}} + \beta^{n+\frac{1}{2}}, \quad i = 1, 2, \tag{3.63}$$

with

$$c_3^{n+1} = 1 - c_1^{n+1} - c_2^{n+1}, \tag{3.64}$$

$$\frac{\mu_3^{n+\frac{1}{2}}}{\Sigma_3} = -\left(\frac{\mu_1^{n+\frac{1}{2}}}{\Sigma_1} + \frac{\mu_2^{n+\frac{1}{2}}}{\Sigma_2} \right). \tag{3.65}$$

Proof. The proof is omitted here since it is similar to that in Theorem 3.1. □

Similar to the first-order scheme, we can rewrite the system (3.59) as follows:

$$\frac{U^{n+1} + U^n}{2} = \frac{1}{2} H_1^{*,n+\frac{1}{2}} c_1^{n+1} + \frac{1}{2} H_2^{*,n+\frac{1}{2}} c_2^{n+1} + \frac{1}{2} H_3^{*,n+\frac{1}{2}} c_3^{n+1} + Q_2^n, \tag{3.66}$$

where $Q_2^n = U^n - \frac{1}{2} H_1^{*,n+\frac{1}{2}} c_1^n - \frac{1}{2} H_2^{*,n+\frac{1}{2}} c_2^n - \frac{1}{2} H_3^{*,n+\frac{1}{2}} c_3^n$. Thus, the system (3.57)–(3.59) can be rewritten as:

$$\frac{c_i^{n+1} - c_i^n}{\delta t} = \frac{M_0}{\Sigma_i} \Delta \mu_i^{n+\frac{1}{2}}, \tag{3.67}$$

$$\begin{aligned} \mu_i^{n+\frac{1}{2}} = &-\frac{3}{8}\epsilon\Sigma_i \Delta c_i^{n+1} + \frac{12}{\epsilon} H_i^{*,n+\frac{1}{2}} \Big(H_1^{*,n+\frac{1}{2}} c_1^{n+1} + H_2^{*,n+\frac{1}{2}} c_2^{n+1} \\ &+ H_3^{*,n+\frac{1}{2}} c_3^{n+1} \Big) + \overline{\beta}^{n+\frac{1}{2}} + h_i^n, \quad i = 1, 2, 3, \end{aligned} \tag{3.68}$$

where

$$\begin{cases} \overline{\beta}^{n+\frac{1}{2}} = -\dfrac{4}{\epsilon}\Sigma_T \displaystyle\sum_{i=1}^{3} \frac{1}{\Sigma_i} H_i^{*,n+\frac{1}{2}} \Big(H_1^{*,n+\frac{1}{2}} c_1^{n+1} + H_2^{*,n+\frac{1}{2}} c_2^{n+1} + H_3^{*,n+\frac{1}{2}} c_3^{n+1} \Big), \\ h_i^n = -\dfrac{3}{8}\epsilon\Sigma_i \Delta c_i^n + \dfrac{24}{\epsilon} H_i^{*,n+\frac{1}{2}} Q_2^n \\ \qquad\quad - \dfrac{8}{\epsilon}\Sigma_T \left(\dfrac{1}{\Sigma_1} H_1^{*,n+\frac{1}{2}} + \dfrac{1}{\Sigma_2} H_2^{*,n+\frac{1}{2}} + \dfrac{1}{\Sigma_3} H_3^{*,n+\frac{1}{2}} \right) Q_2^n. \end{cases}$$

Theorem 3.5. *The linear system given by* (3.67) *and* (3.68) *for variable* $\Phi = (c_1^{n+1}, c_2^{n+1}, c_3^{n+1})^T$ *is self-adjoint and positive definite.*

Proof. The proof is omitted here since it is similar to that of Theorem 3.2. □

The stability result of the second-order Crank–Nicolson scheme (3.57)–(3.59) is given below.

Theorem 3.6. *Assuming* (2.19), *the second-order Crank–Nicolson scheme* (3.57)–(3.59) *is unconditionally energy stable and satisfies the following discrete energy dissipation law*:

$$\begin{aligned}\frac{1}{\delta t}(E_{cn}^{n+1} - E_{cn}^{n}) &= -M_0\left(\frac{1}{\Sigma_1}\left\|\nabla\mu_1^{n+\frac{1}{2}}\right\|^2 + \frac{1}{\Sigma_2}\left\|\nabla\mu_2^{n+\frac{1}{2}}\right\|^2 + \frac{1}{\Sigma_3}\left\|\nabla\mu_3^{n+\frac{1}{2}}\right\|^2\right)\\ &\le -M_0\underline{\Sigma}\left(\frac{\left\|\nabla\mu_1^{n+\frac{1}{2}}\right\|^2}{\Sigma_1^2} + \frac{\left\|\nabla\mu_2^{n+\frac{1}{2}}\right\|^2}{\Sigma_2^2} + \frac{\left\|\nabla\mu_3^{n+\frac{1}{2}}\right\|^2}{\Sigma_3^2}\right), \qquad (3.69)\end{aligned}$$

where E_{cn}^n *that is defined by*

$$\begin{aligned}E_{cn}^n &= \frac{3}{8}\Sigma_1\epsilon\|\nabla c_1^n\|^2 + \frac{3}{8}\Sigma_2\epsilon\|\nabla c_2^n\|^2\\ &\quad + \frac{3}{8}\Sigma_3\epsilon\|\nabla c_3^n\|^2 + \frac{12}{\epsilon}\|U^n\|^2 - \frac{12}{\epsilon}B|\Omega|. \qquad (3.70)\end{aligned}$$

Proof. Taking the L^2-inner product of (3.57) with $-\delta t\mu_i^{n+1}$, we obtain

$$-\left(c_i^{n+1} - c_i^n, \mu_i^{n+\frac{1}{2}}\right) = \delta t\frac{M_0}{\Sigma_i}\left\|\nabla\mu_i^{n+\frac{1}{2}}\right\|^2. \qquad (3.71)$$

Taking the L^2-inner product of (3.58) with $c_i^{n+1} - c_i^n$, we obtain

$$\begin{aligned}\left(\mu_i^{n+\frac{1}{2}}, c_i^{n+1} - c_i^n\right) &= \frac{3}{8}\epsilon\Sigma_i(\|\nabla c_i^{n+1}\|^2 - \|\nabla c_i^n\|^2)\\ &\quad + \frac{24}{\epsilon}\left(H_i^{*,n+\frac{1}{2}}U^{n+\frac{1}{2}}, c_i^{n+1} - c_i^n\right)\\ &\quad + \left(\beta^{n+\frac{1}{2}}, c_i^{n+1} - c_i^n\right). \qquad (3.72)\end{aligned}$$

Taking the L^2-inner product of (3.59) with $\frac{24}{\epsilon}U^{n+\frac{1}{2}}$, we obtain

$$\begin{aligned}&\frac{24}{\epsilon}\Big(\left(H_1^{*,n+\frac{1}{2}}(c_1^{n+1} - c_1^n), U^{n+\frac{1}{2}}\right) + \left(H_2^{*,n+\frac{1}{2}}(c_2^{n+1} - c_2^n), U^{n+\frac{1}{2}}\right)\\ &\quad + \left(H_3^{*,n+\frac{1}{2}}(c_3^{n+1} - c_3^n), U^{n+\frac{1}{2}}\right)\Big)\\ &= \frac{12}{\epsilon}(\|U^{n+1}\|^2 - \|U^n\|^2). \qquad (3.73)\end{aligned}$$

Combining (3.71), (3.72) for $i = 1, 2, 3$ and (3.73), we derive

$$\begin{aligned}
&\frac{3}{8}\epsilon\sum_{i=1}^{3}\Sigma_i\Big(\|\nabla c_i^{n+1}\|^2 - \|\nabla c_i^n\|^2\Big) + \frac{12}{\epsilon}\Big(\|U^{n+1}\|^2 - \|U^n\|^2\Big)\\
&\quad = -M_0\left(\frac{1}{\Sigma_1}\left\|\nabla\mu_1^{n+\frac{1}{2}}\right\|^2 + \frac{1}{\Sigma_1}\left\|\nabla\mu_1^{n+\frac{1}{2}}\right\|^2 + \frac{1}{\Sigma_1}\left\|\nabla\mu_1^{n+\frac{1}{2}}\right\|^2\right)\\
&\quad \le -M_0\Sigma_0\left(\frac{\left\|\nabla\mu_1^{n+\frac{1}{2}}\right\|^2}{\Sigma_1^2} + \frac{\left\|\nabla\mu_2^{n+\frac{1}{2}}\right\|^2}{\Sigma_2^2} + \frac{\left\|\nabla\mu_3^{n+\frac{1}{2}}\right\|^2}{\Sigma_3^2}\right). \qquad (3.74)
\end{aligned}$$

Thus, we obtain the desired result (3.69). □

3.4. *Second-order BDF scheme*

Now we develop another second-order scheme based on the Adam–Bashforth approach (BDF2).

Assuming that $(c_1, c_2, c_3, U)^n$ and $(c_1, c_2, c_3, U)^{n-1}$ are already calculated, we compute $(c_1,\, c_2,\, c_3,\, U)^{n+1}$ from the following discrete system:

$$\frac{3c_i^{n+1} - 4c_i^n + c_i^{n-1}}{2\delta t} = \frac{M_0}{\Sigma_i}\Delta\mu_i^{n+1}, \qquad (3.75)$$

$$\mu_i^{n+1} = -\frac{3}{4}\epsilon\Sigma_i\Delta c_i^{n+1} + \frac{24}{\epsilon}H_i^{\dagger,n+1}U^{n+1} + \beta^{n+1}, \quad i = 1, 2, 3, \qquad (3.76)$$

$$\begin{aligned}
3U^{n+1} - 4U^n + U^{n-1} &= H_1^{\dagger,n+1}(3c_1^{n+1} - 4c_1^n + c_1^{n-1})\\
&\quad + H_2^{\dagger,n+1}(3c_2^{n+1} - 4c_2^n + c_2^{n-1})\\
&\quad + H_3^{\dagger,n+1}(3c_3^{n+1} - 4c_3^n + c_3^{n-1}), \qquad (3.77)
\end{aligned}$$

where

$$\begin{cases}
c_i^\dagger = 2c_i^n - c_i^{n-1},\\
H_1^{\dagger,n+1} = \dfrac{1}{2}\dfrac{\frac{\Sigma_1}{2}\Big(c_1^\dagger - {c_1^\dagger}^2\Big)(1 - 2c_1^\dagger) + 6\Lambda c_1^\dagger {c_2^\dagger}^2 {c_3^\dagger}^2}{\sqrt{F(c_1^\dagger, c_2^\dagger, c_3^\dagger) + B}},\\
H_2^{\dagger,n+1} = \dfrac{1}{2}\dfrac{\frac{\Sigma_2}{2}\Big(c_2^\dagger - {c_2^\dagger}^2\Big)(1 - 2c_2^\dagger) + 6\Lambda {c_1^\dagger}^2 c_2^\dagger {c_3^\dagger}^2}{\sqrt{F(c_1^\dagger, c_2^\dagger, c_3^\dagger) + B}},\\
H_3^{\dagger,n+1} = \dfrac{1}{2}\dfrac{\frac{\Sigma_3}{2}\Big(c_3^\dagger - {c_3^\dagger}^2\Big)(1 - 2c_3^\dagger) + 6\Lambda {c_1^\dagger}^2 {c_2^\dagger}^2 c_3^\dagger}{\sqrt{F(c_1^\dagger, c_2^\dagger, c_3^\dagger) + B}},\\
\beta^{n+1} = -\dfrac{8}{\epsilon}\Sigma_T\left(\dfrac{1}{\Sigma_1}H_1^{\dagger,n+1} + \dfrac{1}{\Sigma_2}H_2^{\dagger,n+1} + \dfrac{1}{\Sigma_3}H_3^{\dagger,n+1}\right)U^{n+1}.
\end{cases} \qquad (3.78)$$

The initial conditions are (3.8) and the boundary conditions are:

$$\text{(i)} \quad \text{all variables are periodic;} \tag{3.79}$$

$$\text{or} \quad \text{(ii)} \quad \partial_{\mathbf{n}} c_i^{n+1}|_{\partial\Omega} = \nabla\mu_i^{n+1} \cdot \mathbf{n}|_{\partial\Omega} = 0, \quad i = 1, 2, 3. \tag{3.80}$$

Similar to the first-order scheme and the second-order Crank–Nicolson scheme, the hyperplane link condition still holds for this scheme.

Theorem 3.7. *System* (3.75)–(3.77) *is equivalent to the following scheme with two-order parameters*:

$$\frac{3c_i^{n+1} - 4c_i^n + c_i^{n-1}}{2\delta t} = \frac{M_0}{\Sigma_i}\Delta\mu_i^{n+1}, \tag{3.81}$$

$$\mu_i^{n+1} = -\frac{3}{4}\epsilon\Sigma_i\Delta c_i^{n+1} + \frac{24}{\epsilon}H_i^{\dagger,n+1}U^{n+1} + \beta^{n+1}, \quad i = 1, 2, \tag{3.82}$$

$$c_3^{n+1} = 1 - c_1^{n+1} - c_2^{n+1}, \tag{3.83}$$

$$\frac{\mu_3^{n+1}}{\Sigma_3} = -\left(\frac{\mu_1^{n+1}}{\Sigma_1} + \frac{\mu_2^{n+1}}{\Sigma_2}\right). \tag{3.84}$$

Proof. The proof is omitted here since it is similar to that of Theorem 3.1. □

Similar to the two previous schemes, we can rewrite the system (3.77) as

$$U^{n+1} = H_1^{\dagger,n+1}c_1^{n+1} + H_2^{\dagger,n+1}c_2^{n+1} + H_3^{\dagger,n+1}c_3^{n+1} + Q_3^n, \tag{3.85}$$

where $Q_3^n = U^{\times,n+1} - H_1^{\dagger,n+1}c_1^{\times,n+1} - H_2^{\dagger,n+1}c_2^{\times,n+1} - H_3^{\dagger,n+1}c_3^{\times,n+1}$ and $S^{\times,n+1} = \frac{4S^n - S^{n-1}}{3}$ for any variable S. Thus, the system (3.75)–(3.77) can be rewritten as:

$$\frac{3c_i^{n+1} - 4c_i^n + c_i^{n-1}}{2\delta t} = \frac{M_0}{\Sigma_i}\Delta\mu_i^{n+1}, \tag{3.86}$$

$$\begin{aligned}\mu_i^{n+1} = &-\frac{3}{4}\epsilon\Sigma_i\Delta c_i^{n+1} + \frac{24}{\epsilon}H_i^{\dagger,n+1}(H_1^{\dagger,n+1}c_1^{n+1} + H_2^{\dagger,n+1}c_2^{n+1} \\ &+ H_3^{\dagger,n+1}c_3^{n+1}) + \overline{\beta}^{n+1} + f_i^n, \quad i = 1, 2, 3,\end{aligned} \tag{3.87}$$

where

$$\begin{cases}\overline{\beta}^{n+1} = -\dfrac{8}{\epsilon}\Sigma_T\left(\dfrac{1}{\Sigma_1}H_1^{\dagger,n+1} + \dfrac{1}{\Sigma_2}H_2^{\dagger,n+1} + \dfrac{1}{\Sigma_3}H_3^{\dagger,n+1}\right) \\ \qquad\qquad \times (H_1^{\dagger,n+1}c_1^{n+1} + H_2^{\dagger,n+1}c_2^{n+1} + H_3^{\dagger,n+1}c_3^{n+1}), \\ f_i^n = \dfrac{24}{\epsilon}H_i^{\dagger,n+1}Q_3^n - \dfrac{8}{\epsilon}\Sigma_T\left(\dfrac{1}{\Sigma_1}H_1^{\dagger,n+1} + \dfrac{1}{\Sigma_2}H_2^{\dagger,n+1} + \dfrac{1}{\Sigma_3}H_3^{\dagger,n+1}\right)Q_3^n.\end{cases}$$

Theorem 3.8. *The linear system given by* (3.86)–(3.87) *for variable* $\Phi = (c_1^{n+1}, c_2^{n+1}, c_3^{n+1})^T$ *is self-adjoint and positive definite.*

Proof. The proof is omitted here since it is similar to that of Theorem 3.2. □

Theorem 3.9. *The second-order scheme given by* (3.75)–(3.77) *is unconditionally energy stable and satisfies the following discrete energy dissipation law*:

$$\frac{1}{\delta t}(E_{bdf}^{n+1} - E_{bdf}^{n}) \le -M_0 \left(\frac{1}{\Sigma_1}\|\nabla \mu_1^{n+1}\|^2 + \frac{1}{\Sigma_2}\|\nabla \mu_2^{n+1}\|^2 + \frac{1}{\Sigma_3}\|\nabla \mu_3^{n+1}\|^2 \right)$$
$$\le -M_0 \underline{\Sigma} \left(\frac{\|\nabla \mu_1^{n+1}\|^2}{\Sigma_1^2} + \frac{\|\nabla \mu_2^{n+1}\|^2}{\Sigma_2^2} + \frac{\|\nabla \mu_3^{n+1}\|^2}{\Sigma_3^2} \right), \tag{3.88}$$

where E_{bdf}^n *is defined by*

$$E_{bdf}^n = \frac{3}{8}\Sigma_1 \epsilon \left(\frac{\|\nabla c_1^n\|^2}{2} + \frac{\|2\nabla c_1^n - \nabla c_1^{n-1}\|^2}{2} \right)$$
$$+ \frac{3}{8}\Sigma_2 \epsilon \left(\frac{\|\nabla c_2^n\|^2}{2} + \frac{\|2\nabla c_2^n - \nabla c_2^{n-1}\|^2}{2} \right)$$
$$+ \frac{3}{8}\Sigma_3 \epsilon \left(\frac{\|\nabla c_3^n\|^2}{2} + \frac{\|2\nabla c_3^n - \nabla c_3^{n-1}\|^2}{2} \right)$$
$$+ \frac{12}{\epsilon} \left(\frac{\|U^n\|^2}{2} + \frac{\|2U^n - U^{n-1}\|^2}{2} \right) - \frac{12}{\epsilon} B|\Omega|. \tag{3.89}$$

Proof. Taking the L^2-inner product of (3.75) with $-2\delta t \mu_i^{n+1}$, we obtain

$$-(3c_i^{n+1} - 4c_i^n + c_i^{n-1}, \mu_i^{n+1}) = 2\delta t \frac{M_0}{\Sigma_i}\|\nabla \mu_i^{n+1}\|^2. \tag{3.90}$$

Taking the L^2-inner product of (3.76) with $3c_i^{n+1} - 4c_i^n + c_i^{n-1}$, and applying the following identity

$$2(3a - 4b + c, a) = |a|^2 - |b|^2 + |2a - b|^2 - |2b - c|^2 + |a - 2b + c|^2, \tag{3.91}$$

we derive

$$(\mu_i^{n+1}, 3c_i^{n+1} - 4c_i^n + c_i^{n-1})$$
$$= \frac{3}{8}\epsilon \Sigma_i (\|\nabla c_i^{n+1}\|^2 - \|\nabla c_i^n\|^2 + \|2\nabla c_i^{n+1} - \nabla c_i^n\|^2 - \|2\nabla c_i^n - \nabla c_i^{n-1}\|^2)$$
$$+ \frac{3}{8}\epsilon \Sigma_i \|\nabla c_i^{n+1} - 2\nabla c_i^n + \nabla c_i^{n-1}\|^2$$
$$+ \frac{24}{\epsilon}(H_i^{\dagger, n+1} U^{n+1}, 3c_i^{n+1} - 4c_i^n + c_i^{n-1})$$
$$+ (\beta^{n+1}, 3c_i^{n+1} - 4c_i^n + c_i^{n-1}). \tag{3.92}$$

Taking the L^2-inner product of (3.77) with $\frac{24}{\epsilon}U^{n+1}$, we obtain

$$\begin{aligned}
&\frac{12}{\epsilon}(\|U^{n+1}\|^2-\|U^n\|^2+\|2U^{n+1}-U^n\|^2-\|2U^n-U^{n-1}\|^2\\
&\qquad+\|U^{n+1}-2U^n+U^{n-1}\|^2)\\
&\quad=\frac{24}{\epsilon}((H_1^{\dagger,n+1}(3c_1^{n+1}-4c_1^n+c_1^{n-1}),U^{n+1})\\
&\qquad+(H_2^{\dagger,n+1}(3c_2^{n+1}-4c_2^n+c_2^{n-1}),U^{n+1})\\
&\qquad+(H_3^{\dagger,n+1}(3c_3^{n+1}-4c_3^n+c_3^{n-1}),U^{n+1})).
\end{aligned}\tag{3.93}$$

Combining (3.90), (3.92) for $i=1,2,3$ and (3.93), we derive

$$\begin{aligned}
&\frac{3}{8}\epsilon\sum_{i=1}^{3}\Sigma_i(\|\nabla c_i^{n+1}\|^2+\|2\nabla c_i^{n+1}-\nabla c_i^n\|^2)\\
&\qquad-\frac{3}{8}\epsilon\sum_{i=1}^{3}\Sigma_i(\|\nabla c_i^n\|^2+\|2\nabla c_i^n-\nabla c_i^{n-1}\|^2)\\
&\qquad+\frac{3}{8}\epsilon\sum_{i=1}^{3}\Sigma_i(\|\nabla c_i^{n+1}-2\nabla c_i^n+\nabla c_i^{n-1}\|^2)\\
&\qquad+\frac{12}{\epsilon}(\|U^{n+1}\|^2+\|2U^{n+1}-U^n\|^2)\\
&\qquad-\frac{12}{\epsilon}(\|U^n\|^2+\|2U^n-U^{n-1}\|^2)+\frac{12}{\epsilon}\|U^{n+1}-2U^n+U^{n-1}\|^2\\
&\quad=-2\delta t M_0\left(\frac{1}{\Sigma_1}\|\nabla\mu_1^{n+1}\|^2+\frac{1}{\Sigma_2}\|\nabla\mu_2^{n+1}\|^2+\frac{1}{\Sigma_3}\|\nabla\mu_3^{n+1}\|^2\right)\\
&\quad\le-2\delta t M_0\underline{\Sigma}\left(\frac{\|\nabla\mu_1^{n+1}\|^2}{\Sigma_1^2}+\frac{\|\nabla\mu_2^{n+1}\|^2}{\Sigma_2^2}+\frac{\|\nabla\mu_3^{n+1}\|^2}{\Sigma_3^2}\right).
\end{aligned}\tag{3.94}$$

Since $\sum_{i=1}^{3}(\nabla c_i^{n+1}-2\nabla c_i^n+\nabla c_i^{n-1})=0$, from Lemma 2.1, we have

$$\begin{aligned}
&\sum_{i=1}^{3}\{\Sigma_i\|\nabla c_i^{n+1}-2\nabla c_i^n+\nabla c_i^{n-1}\|^2\}\\
&\qquad\ge\underline{\Sigma}\sum_{i=1}^{3}\{\|\nabla c_i^{n+1}-2\nabla c_i^n+\nabla c_i^{n-1}\|^2\}\ge 0.
\end{aligned}\tag{3.95}$$

Therefore, we obtain (3.88) after we drop the unnecessary positive terms in (3.94).

□

Remark 3.7. From formal Taylor expansion, we find

$$\left(\frac{\|\phi^{n+1}\|^2+\|2\phi^{n+1}-\phi^n\|^2}{2\delta t}\right)-\left(\frac{\|\phi^n\|^2+\|2\phi^n-\phi^{n-1}\|^2}{2\delta t}\right)$$
$$\cong\left(\frac{\|\phi^{n+2}\|^2-\|\phi^n\|^2}{2\delta t}\right)+O(\delta t^2)\cong\frac{d}{dt}\|\phi(t^{n+1})\|^2+O(\delta t^2),\quad(3.96)$$

and

$$\frac{\|\phi^{n+1}-2\phi^n+\phi^{n-1}\|^2}{\delta t}\cong O(\delta t^3)\quad(3.97)$$

for any variable ϕ. Therefore, the discrete energy law (3.88) is a second-order approximation of $\frac{d}{dt}E^{\text{triph}}(\phi)$ in (3.11).

4. Numerical Simulations

We present in this section several 2D and 3D numerical examples using the schemes constructed in the previous section. The computational domain is $\Omega=(0,1)^d$, $d=2,3$. We use the central finite difference method to discretize the spatial derivatives with 128^d grid points in all simulations.

Unless otherwise explicitly specified, the default parameter values are:

$$\epsilon=0.03,\quad B=2,\quad M_0=10^{-6},\quad \Lambda=7.\quad(4.1)$$

Remark 4.1. Parameter B is chosen to ensure that $F(c_1,c_2,c_3)+B$ is always positive. For the partial spreading case, since $\Sigma_i>0$, $\forall\, i=1,2,3$, we can choose $B=0$. For the total spreading case, we usually choose B large enough. But we remark that the computed solutions are not sensitive with the choice of B.

4.1. *Accuracy test*

For convenience, we denote first-order scheme (3.12)–(3.14) by LS1, second-order scheme (3.57)–(3.59) by LS2-CN, scheme (3.75)–(3.77) by LS2-BDF.

We set the initial condition as follows:

$$\begin{cases} c_3=\dfrac{1}{2}\left(1+\tanh\left(\dfrac{R-0.15}{\epsilon}\right)\right),\\ c_1=\dfrac{1}{2}(1-c_3)\left(1+\tanh\left(\dfrac{y-0.5}{\epsilon}\right)\right),\\ c_2=1-c_1-c_3, \end{cases}\quad(4.2)$$

where $R=\sqrt{(x-0.5)^2+(y-0.5)^2}$. Since the exact solutions are not known, we compute the errors by adjacent time step. We present the summations of the L^2-, L^1- and L^∞-errors of the three-phase variables at $t=1$ with different time step sizes in Tables 1–3 for the three proposed schemes. We observe that schemes LS1, LS2-CN and LS2-BDF asymptotically match the first-order and second-order accuracy in time, respectively.

Table 1. The L^2-, L^1-, L^∞-numerical errors at $t = 1$ that are computed by the first-order scheme LS1 using various temporal resolutions. The order parameters are of (4.1) and 128^2 grid points are used to discretize the space.

Coarse δt	Fine δt	L^2-Error	Order	L^1-Error	Order	L^∞-Error	Order
0.01	0.005	7.120e-3	—	3.969e-1	—	3.950e-4	—
0.005	0.0025	3.816e-3	0.90	2.112e-1	0.91	2.067e-4	0.93
0.0025	0.00125	1.999e-3	0.93	1.101e-1	0.94	1.062e-4	0.96
0.00125	0.000625	1.028e-3	0.96	5.645e-2	0.96	5.395e-5	0.98
0.000625	0.0003125	5.225e-4	0.98	2.863e-2	0.98	2.719e-5	0.99
0.0003125	0.00015625	2.635e-4	0.99	1.442e-2	0.99	1.365e-5	0.99
0.00015625	0.000078125	1.323e-4	0.99	7.239e-3	0.99	6.842e-6	1.0

Table 2. The L^2-, L^1-, L^∞-numerical errors at $t = 1$ that are computed by the second-order scheme LS2-CN using various temporal resolutions. The order parameters are of (4.1) and 128^2 grid points are used to discretize the space.

Coarse δt	Fine δt	L^2-Error	Order	L^1-Error	Order	L^∞-Error	Order
0.01	0.005	3.636e-3	—	1.541e-1	—	2.460e-4	—
0.005	0.0025	1.205e-3	1.59	4.972e-2	1.63	9.311e-5	1.40
0.0025	0.00125	3.590e-4	1.75	1.453e-2	1.78	2.999e-5	1.63
0.00125	0.000625	9.936e-5	1.85	3.941e-3	1.88	8.653e-6	1.79
0.000625	0.0003125	2.626e-5	1.92	1.030e-3	1.93	2.336e-6	1.89
0.0003125	0.00015625	6.759e-6	1.96	2.636e-4	1.97	6.080e-7	1.94
0.00015625	0.000078125	1.715e-7	1.98	6.671e-5	1.98	1.551e-7	1.97

Table 3. The L^2-, L^1-, L^∞-numerical errors at $t = 1$ that are computed by the second-scheme LS2-BDF using various temporal resolutions. The order parameters are of (4.1) and 128^2 grid points are used to discretize the space.

Coarse δt	Fine δt	L^2-Error	Order	L^1-Error	Order	L^∞-Error	Order
0.01	0.005	6.368e-3	—	5.374e-1	—	5.018e-4	—
0.005	0.0025	2.584e-3	1.30	2.143e-1	1.33	1.811e-4	1.47
0.0025	0.00125	9.528e-4	1.44	7.588e-2	1.50	5.836e-5	1.63
0.00125	0.000625	3.172e-4	1.59	2.443e-2	1.64	2.244e-5	1.38
0.000625	0.0003125	9.641e-5	1.72	7.488e-3	1.71	7.170e-6	1.65
0.0003125	0.00015625	2.626e-5	1.88	2.095e-3	1.84	1.955e-6	1.87
0.00015625	0.000078125	7.012e-6	1.91	6.424e-4	1.70	5.099e-7	1.94

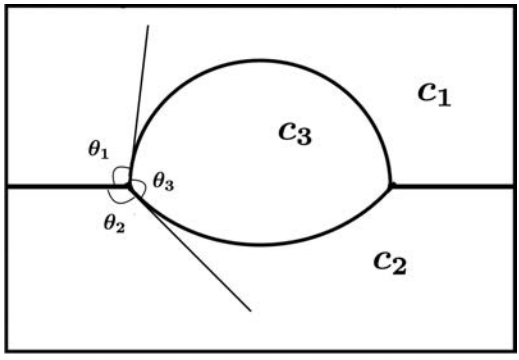

Fig. 1. Theoretical shape of the contact lens at the equilibrium between two stratified fluid components.

4.2. *Liquid lens between two stratified fluids*

We start by recomputing two examples presented in Figs. 11 and 19 in Ref. 7 using the same parameter values as in Ref. 7 with the initial condition set as follows:

$$\begin{aligned} c_1^0(\mathbf{x}) &= \frac{1}{2}\left(1+\tanh\left(\frac{2}{\epsilon}\min(|\mathbf{x}|-0.1,\mathrm{y})\right)\right),\\ c_2^0(\mathbf{x}) &= \frac{1}{2}\left(1-\tanh\left(\frac{2}{\epsilon}\min(-|\mathbf{x}|+0.1,\mathrm{y})\right)\right),\\ c_3^0(\mathbf{x}) &= 1-c_1^0(\mathbf{x})-c_2^0(\mathbf{x}). \end{aligned} \tag{4.3}$$

The order parameters are $\epsilon = 10^{-2},\ M_0 = 10^{-4}$. In Fig. 2, we set $\sigma_{12} = 1,\ \sigma_{13} = 0.8,\ \sigma_{23} = 1.4$, we observe that the partial spreading phenomena are qualitatively consistent to Fig. 11 in Ref. 7. In Fig. 3, we set $\sigma_{12} = 3, \sigma_{13} = 1, \sigma_{23} = 1$, we observe that the total spreading phenomena are qualitatively consistent to Fig. 16 in Ref. 7. The energy evolution curves for these two simulations are shown in Fig. 4. The quantitative differences between our energy curves presented in Fig. 4 and theirs in Figs. 13 and 19 in Ref. 7 are possible due to the different orders of accuracy of the schemes used: ours is second-order in time while theirs is first-order in time.

Next, we conduct simulations for the classical test case of a liquid lens that is initially spherical, sitting at the interface between two other phases. For the

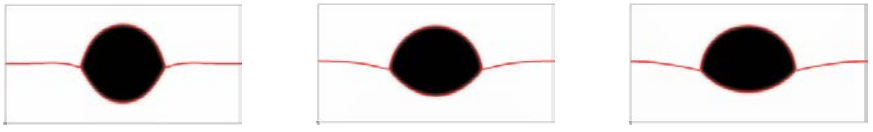

Fig. 2. (Color online) The dynamical behaviors of the liquid lens between two stratified fluids for the partial spreading case. Snapshots are taken at $t = 0.2, 2, 5$. The initial condition is (4.3), the surface tension parameters are $\sigma_{12} = 1, \sigma_{13} = 0.8, \sigma_{23} = 1.4$, the time step is $\delta t = 10^{-4}$ and the grid points are 128^2. The color in black (upper half), white (lower half) and red circle (lens) represent fluids I, II and III, respectively.

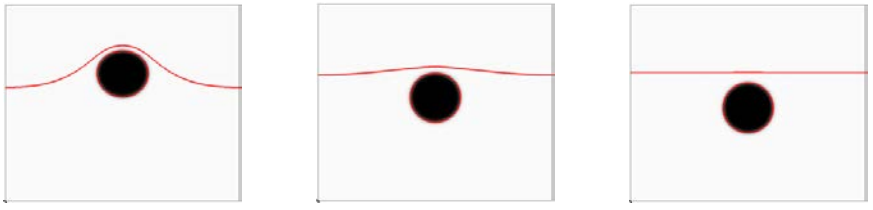

Fig. 3. (Color online) The dynamical behaviors of the liquid lens between two stratified fluids for the total spreading case (no junction points). Snapshots are taken at $t = 2, 30, 300$. The initial condition is (4.3), the surface tension parameters are $\sigma_{12} = 3, \sigma_{13} = 1, \sigma_{23} = 1$, the time step is $\delta t = 10^{-4}$, and the grid points are 128^2. The color in black (upper half), white (lower half) and red circle (lens) represent fluids I, II and III, respectively.

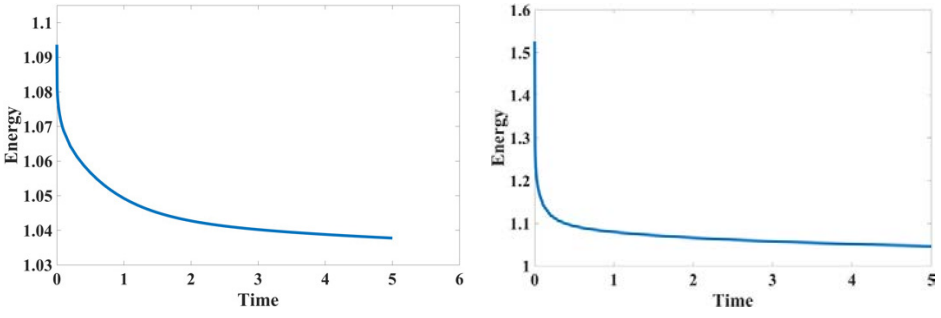

(a) (b)

Fig. 4. Time evolution of the free energy functional for the partial spreading case and total spreading case with initial condition (4.3). The surface tension parameters are: (a) $\sigma_{12} = 1,\ \sigma_{13} = 0.8,\ \sigma_{23} = 1.4$; (b) $\sigma_{12} = 3,\ \sigma_{13} = 1,\ \sigma_{23} = 1$.

accuracy reason, we always use the second-order scheme LS2-CN and take time step $\delta t = 0.001$.

The equilibrium state in the limit $\epsilon \to 0$ can be computed analytically: the final shape of the lens is the union of two pieces of circles, the contact angles being given as a function of the three surface tensions by the Young's relations as shown in Fig. 1 (cf. Refs. 6, 28 and 40):

$$\frac{\sin\theta_1}{\sigma_{23}} = \frac{\sin\theta_2}{\sigma_{13}} = \frac{\sin\theta_3}{\sigma_{12}}. \tag{4.4}$$

We still use the initial condition in the previous example, as shown in the first subfigure in Figs. 2–6, in which, the initial contact angles are $\theta_1 = \theta_2 = \frac{\pi}{2}$ and $\theta_3 = \pi$.

We first simulate the case of partial spreading. In Fig. 2(a), we set the three surface tension parameter values as $\sigma_{12} = \sigma_{13} = \sigma_{23} = 1$, we observe that the three contact angles finally become $\frac{2\pi}{3}$ for all, shown in the final subfigure of Fig. 2 because the surface tension force between each phase is the same, which is consistent to the theoretical values of sharp interface from (4.4). In Fig. 2(b), we keep $\sigma_{12} = 1$ and decrease the other two parameter values as $\sigma_{13} = \sigma_{23} = 0.6$. From the contact angle formulation (4.4), we have $\theta_1 = \theta_2 > \theta_3$, which is confirmed by the numerical results shown in Fig. 2(b). We further vary the two surface tension parameter values σ_{13} and σ_{23} to be 0.8 and 1.4, respectively while keeping $\sigma_{12} = 1$ in Fig. 5(c). After the intermediate dynamical adjustment, the contact angles at equilibrium become $\theta_1 < \theta_3 < \theta_2$, which is consistent to the formulation (4.4) as well.

We then simulate the case of total spreading (without a junction point) in Fig. 6. We set the three surface tension parameter values as $\sigma_{12} = 3,\ \sigma_{13} = 1,\ \sigma_{23} = 1$. From (4.4), the three contact angles can be computed as $\theta_1 = \theta_2 = \pi$ and $\theta_3 = 0$, that can be observed in Fig. 6(a), where the third fluid component c_3 totally spreads to a layer. For the final case, we set $\sigma_{12} = 1, \sigma_{13} = 1, \sigma_{23} = 3$. By (4.4), it can be computed that the three contact angles at equilibrium are $\theta_1 = 0,\ \theta_2 = \theta_3 = \pi$,

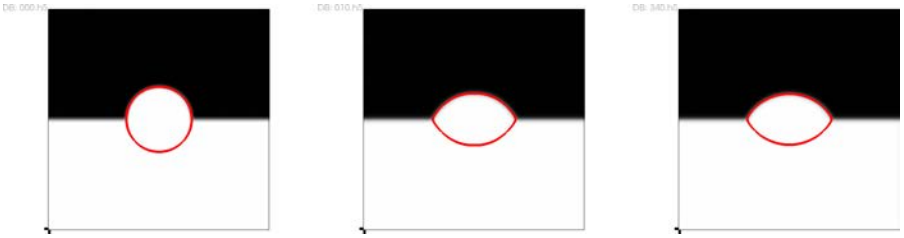

(a) $(\sigma_{12};\sigma_{13};\sigma_{23}) = (1;1;1)$.

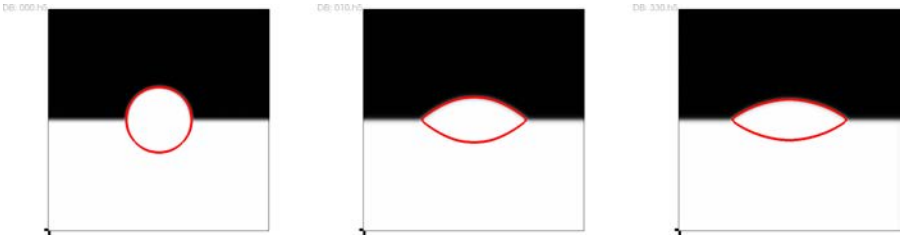

(b) $(\sigma_{12};\sigma_{13};\sigma_{23}) = (1;0.6;0.6)$.

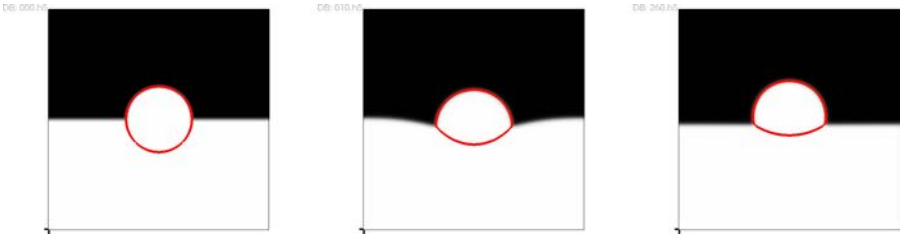

(c) $(\sigma_{12};\sigma_{13};\sigma_{23}) = (1;0.8;1.4)$.

Fig. 5. (Color online) The dynamical behaviors until the steady state of a liquid lens between two stratified fluids for the partial spreading case, with three sets of different surface tension parameters $\sigma_{12}, \sigma_{13}, \sigma_{23}$, where the time step is $\delta t = 0.001$ and 128^2 grid points are used. The color in black (upper half), white (lower half) and red circle (lens) represent fluids I, II and III, respectively.

which indicates that the first and third fluid components c_1, c_3 are totally spread, and c_2 stays inside the first fluid component, as shown in Fig. 6(b). We remark that all numerical results are qualitatively consistent with the computation results obtained in Refs. 6 and 30.

4.3. *Spinodal decomposition in* 2D

In this example, we study phase separation behavior, i.e. the so-called the spinodal decomposition phenomenon. The process of the phase separation can be studied by considering a homogeneous binary mixture, which is quenched into the unstable part of its miscibility gap. In this case, the spinodal decomposition takes place,

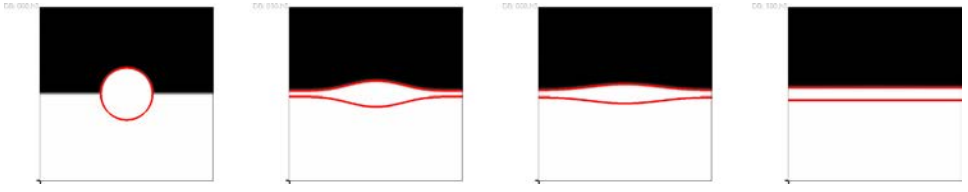

(a) $(\sigma_{12};\sigma_{13};\sigma_{23}) = (3;1;1)$.

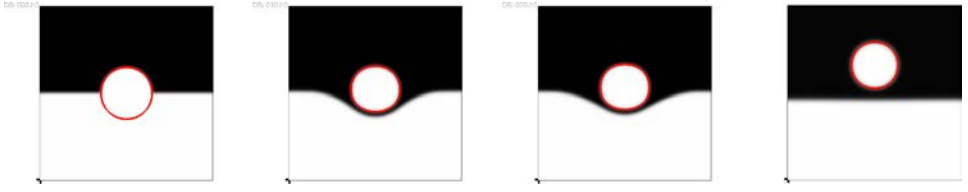

(b) $(\sigma_{12};\sigma_{13};\sigma_{23}) = (1;1;3)$.

Fig. 6. (Color online) The dynamical behaviors until the steady state of a liquid lens between two stratified fluids for the total spreading case (no junction points), with two sets of different surface tension parameters $\sigma_{12}, \sigma_{13}, \sigma_{23}$, where the time step is $\delta t = 0.001$ and 128^2 grid points are used. The color in black (upper half), white (lower half) and red circle (lens) represent fluids I, II and III, respectively.

which manifests in the spontaneous growth of the concentration fluctuations that leads the system from the homogeneous to the two phase state. Shortly after the phase separation starts, the domains of the binary components are formed and the interface between different phases can be specified.[4,13,76] For the accuracy reason, we use the second-order scheme LS2-CN and take the time step $\delta t = 0.001$.

The initial condition is taken as the randomly perturbed concentration field as follows:

$$\phi_i = 0.5 + 0.001\ \mathrm{rand}(x, y), \quad c_i|_{(t=0)} = \frac{\phi_i}{\phi_1 + \phi_2 + \phi_3}, \quad i = 1, 2, 3, \tag{4.5}$$

where the $\mathrm{rand}(x, y)$ is the random number in $[-1, 1]$ which has a zero mean. To label the three phases, we use pink, gray and yellow to represent phases I, II and III respectively.

In Fig. 7, we conduct numerical simulations for the case of order parameters $\sigma_{12} = \sigma_{13} = \sigma_{23} = 1$ as Fig. 2(a). We observe the phase separation behavior and the final equilibrium solution $t = 30{,}000$ present a very regular shape where the three contact angles are $\theta_1 = \theta_2 = \theta_3 = \frac{2\pi}{3}$. In Fig. 8 with the same initial condition, we set the surface tension parameter values as $\sigma_{12} = 1, \sigma_{13} = 0.8, \sigma_{23} = 1.4$. The final equilibrium solution after $t = 30{,}000$ shows three different contact angles that obey $\theta_1 < \theta_3 < \theta_2$, consistent to the example Fig. 5(c). The total spreading case is simulated in Fig. 9, in which we set the surface tension parameter values as $\sigma_{12} = 1, \sigma_{13} = 1, \sigma_{23} = 3$. The final equilibrium solution after $t = 30{,}000$ presents that not a junction point appears, similar to Fig. 6(b).

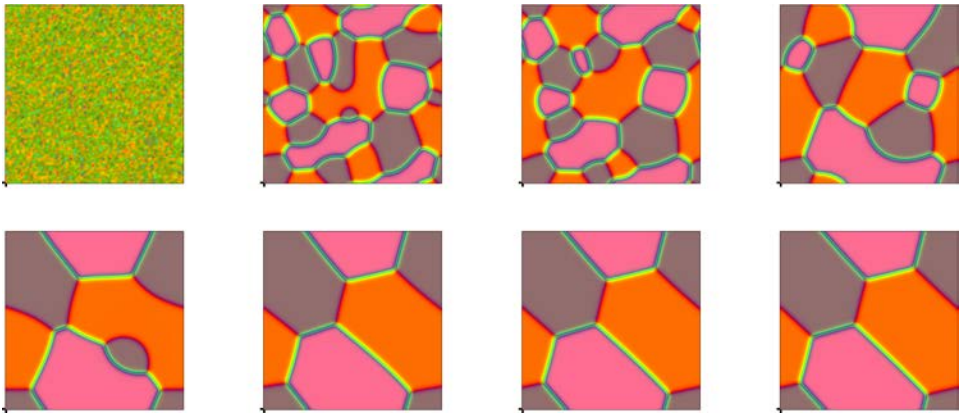

Fig. 7. (Color online) The 2D dynamical evolution of the three-phase variables $c_i, i = 1, 2, 3$ for the partial spreading case, where order parameters are $(\sigma_{12}; \sigma_{13}; \sigma_{23}) = (1 : 1 : 1)$, the time step is $\delta t = 0.001$ and 128^2 grid points are used. Snapshots of the numerical approximation are taken at $t = 0, 1000, 2000, 5000, 10{,}000, 20{,}000, 25{,}000, 30{,}000$. The color in pink, gray and yellow represents the three phases I, II and III, respectively.

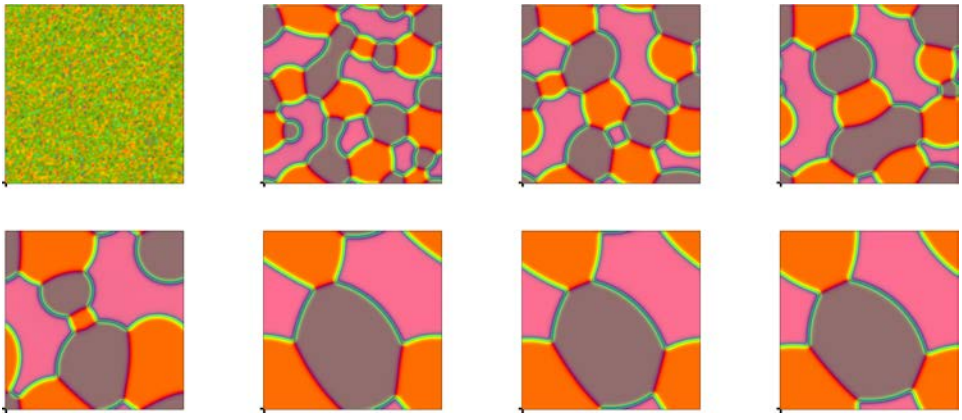

Fig. 8. (Color online) The 2D dynamical evolution of the three-phase variables $c_i, i = 1, 2, 3$ for the partial spreading case, where the order parameters are $(\sigma_{12}; \sigma_{13}; \sigma_{23}) = (1, 0.8, 1.4)$, the time step is $\delta t = 0.001$ and 128^2 grid points are used. Snapshots of the numerical approximation are taken at $t = 0$, 1000, 2000, 5000, 10,000, 20,000, 25,000, 30,000. The color in pink, gray and yellow represents the three phases I, II and III, respectively.

In Fig. 10, we present the evolution of the free energy functional for all three cases. The energy curves show the decay with time that confirms that our algorithms are unconditionally stable. In particular, we plot the time evolution of the free energy with different time steps. It verifies that our numerical scheme predicts accurate results with relative large time steps. The corresponding total CPU/GPU time spent (in seconds) to calculate until $t_{\max} = 500$ with various time steps $\delta t = 10^{-2}, 5 \times 10^{-3}, 2.5 \times 10^{-3}, 1.25 \times 10^{-3}$ are listed in Table 4.

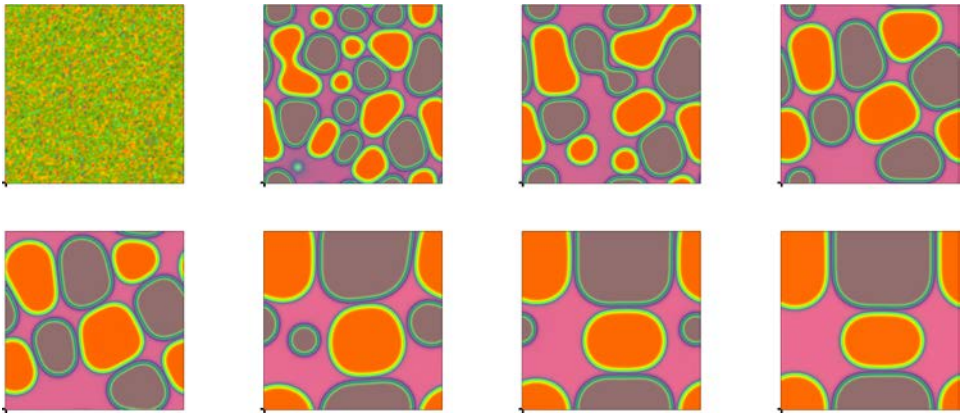

Fig. 9. The 2D dynamical evolution of the three-phase variable c_i for the total spreading case (no junction points), where the order parameters are $(\sigma_{12};\sigma_{13};\sigma_{23}) = (1,1,3)$, the time step is $\delta t = 0.001$ and 128^2 grid points are used. Snapshots of the numerical approximation are taken at $t = 0, 1000, 2000, 5000, 10{,}000, 20{,}000, 25{,}000, 30{,}000$. The color in pink, gray and yellow represents the three phases I, II and III, respectively.

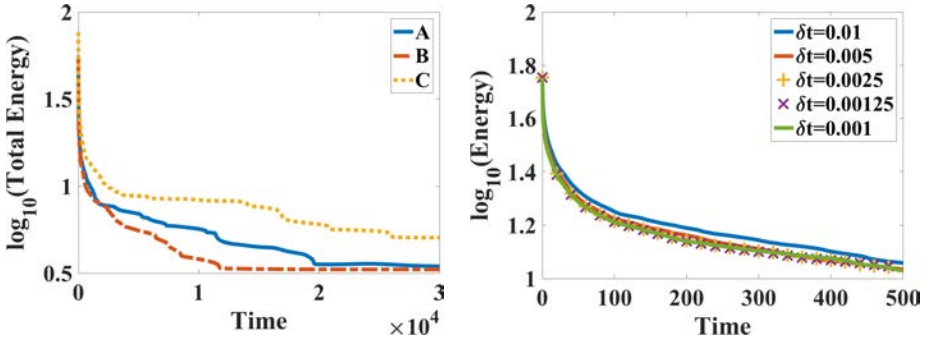

(a) (b)

Fig. 10. (a) Time evolution of the free energy functional using the algorithm LS2-CN using $\delta t = 0.001$ for the three-order parameter set of $A : (\sigma_{12};\sigma_{13};\sigma_{23}) = (1, 0.8, 1.4)$ (partial spreading), $B : (\sigma_{12};\sigma_{13};\sigma_{23}) = (1,1,1)$ (partial spreading), and $C : (\sigma_{12};\sigma_{13};\sigma_{23}) = (1,1,3)$ (total spreading). The x-axis is time, and y-axis is $\log_{10}$(total energy). (b) Time evolution of the free energy with different time steps for Case B.

Table 4. Total CPU/GPU time (in seconds) with various time steps to $t_{\max} = 500$.

Time step δt	1e-2	5e-3	2.5e-3	1.25e-3
Total CPU/GPU time	464 s	732 s	1081 s	1608 s

4.4. *Spinodal decomposition in* 3D

Finally, we present 3D simulations of phase separation dynamics using second-order scheme LS2-CN and time step $\delta t = 0.001$. In order to be consistent with the 2D case, the initial condition is set as follows:

$$\phi_i = 0.5 + 0.001 \text{ rand}(x, y, z), \quad c_i|_{(t=0)} = \frac{\phi_i}{\phi_1 + \phi_2 + \phi_3}, \quad i = 1, 2, 3, \quad (4.6)$$

where the rand(x, y, z) is the random number in $[-1, 1]$ with a zero mean.

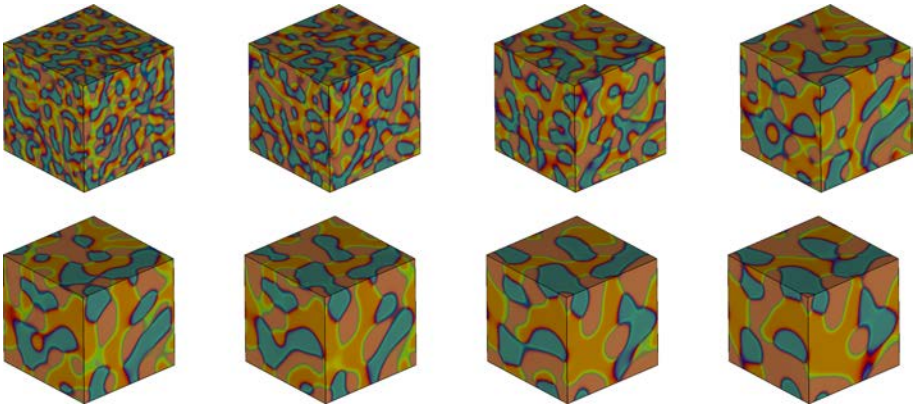

Fig. 11. The 3D dynamical evolution of the three-phase variables c_i, $i = 1, 2, 3$ for the partial spreading case, where the order parameters are $(\sigma_{12}; \sigma_{13}; \sigma_{23}) = (1:1:1)$ and time step is $\delta t = 0.001$. 128^3 grid points are used to discretize the space. Snapshots of the numerical approximation are taken at $t = 50, 100, 200, 500, 750, 1000, 1500, 2000$. The color in pink, gray and yellow represents the three phases I, II and III, respectively.

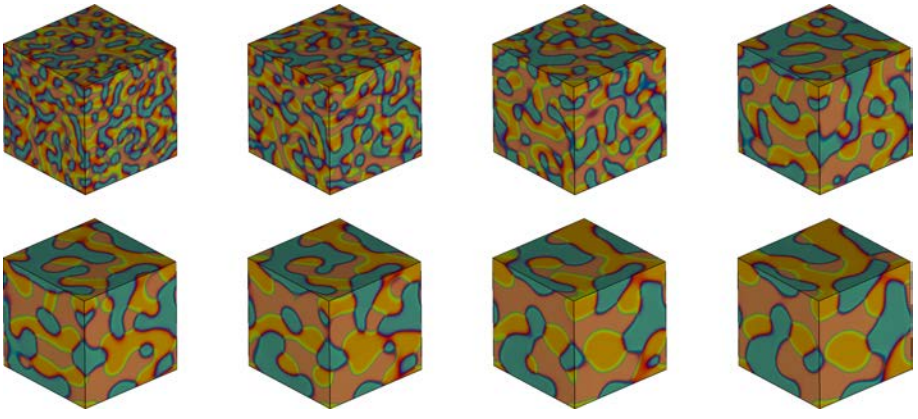

Fig. 12. The 3D dynamical evolution of the three-phase variable c_i, $i = 1, 2, 3$ for the partial spreading case, where the order parameters are $(\sigma_{12}; \sigma_{13}; \sigma_{23}) = (1:0.8:1.4)$ and time step is $\delta t = 0.001$. 128^3 grid points are used to discretize the space. Snapshots of the numerical approximation are taken at $t = 50, 100, 200, 500, 750, 1000, 1500, 2000$. The color in pink, gray and yellow represents the three phases I, II and III, respectively.

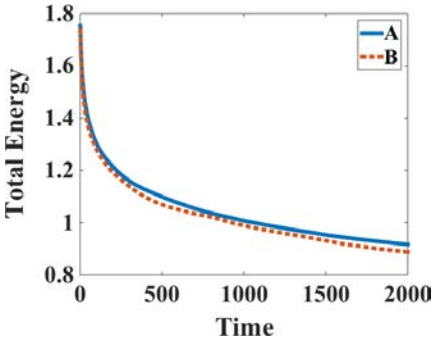

Fig. 13. Time evolution of the free energy functional using the algorithm LS2-CN using $\delta t = 0.001$ for the three-order parameter set of $A : (\sigma_{12}; \sigma_{13}; \sigma_{23}) = (1, 0.8, 1.4)$ and $B : (\sigma_{12}; \sigma_{13}; \sigma_{23}) = (1, 1, 1)$. The x-axis is time, and y-axis is $\log_{10}$(total energy).

Figure 11 shows the dynamical behavior of phase separation for three equal surface tension parameter values $\sigma_{12} = \sigma_{13} = \sigma_{23} = 1$. In Fig. 12, we set the surface tension parameter values as $\sigma_{12} = 1,\ \sigma_{13} = 0.8,\ \sigma_{23} = 1.4$. We observe that the three components accumulate but with different contact angles, consistent to the 2D case. In Fig. 13, we depict the evolution of the free energy functional, in which the energy curves show decays with time.

5. Concluding Remarks

We develop in this paper several efficient time stepping schemes for a three-component Cahn–Hilliard phase-field model that are linear and unconditionally energy stable based on a novel IEQ approach. The proposed schemes bypass the difficulties encountered in the convex splitting and the stabilized approach and enjoy the following desirable properties: (i) *accurate* (up to second-order in time); (ii) *unconditionally energy stable*; and (iii) *easy to implement* (one only solves linear equations at each time step). Moreover, the resulting linear system at each time step is symmetric, positive definite so that it can be efficiently solved by any Krylov subspace methods with suitable (e.g. block-diagonal) pre-conditioners.

To the best of our knowledge, these new schemes are the first schemes that are linear and unconditionally energy stable for the three-component Cahn–Hilliard phase-field model. These schemes can be applied to the hydrodynamically coupled three-phase model without essential difficulties. Although we considered only time discretization in this study, it is expected that similar results can be established for a large class of consistent finite-dimensional Galerkin approximations since the proofs are all based on a variational formulation with all test functions in the same space as the space of the trial functions.

Acknowledgments

X.Y. research is partially supported by the US National Science Foundation under grant numbers DMS-1200487 and DMS-1418898. Q.W. research is partially

supported by grants of the US National Science Foundation under grant numbers DMS-1200487 and DMS-1517347, and a grant from the National Science Foundation of China under the grant number NSFC-11571032. J.S. research is partially supported by the US National Science Foundation under Grants DMS-1419053, DMS-1620262 and AFOSR Grant FA9550-16-1-0102.

References

1. D. M. Anderson, G. B. McFadden and A. A. Wheeler, Diffuse-interface methods in fluid mechanics, *Ann. Rev. Fluid Mech.* **30** (1998) 139–165.
2. J. W. Barrett and J. F. Blowey, An improved error bound for a finite element approximation of a model for phase separation of a multi-component alloy, *IMA J. Numer. Anal.* **19** (1999) 147–168.
3. J. W. Barrett, J. F. Blowey and H. Garcke, On fully practical finite element approximations of degenerate Cahn–Hilliard systems, *ESAIM*: *M2AN* **35** (2001) 713–748.
4. K. Binder, Collective diffusion, nucleation and spinodal decomposition in polymer mixtures, *J. Chem. Phys.* **79** (1983) 6387–6409.
5. J. F. Blowey, M. I. M. Copetti and C. M. Elliott, Numerical analysis of a model for phase separation of a multi-component alloy, *IMA J. Numer. Anal.* **16** (1996) 111–139.
6. F. Boyer and C. Lapuerta, Study of a three-component Cahn–Hilliard flow model, *ESAIM*: *M2AN* **40** (2006) 653–687.
7. F. Boyer and S. Minjeaud, Numerical schemes for a three-component Cahn–Hilliard model, *ESAIM*: *M2AN* **45** (2011) 697–738.
8. G. Caginalp and X. Chen, Convergence of the phase-field model to its sharp interface limits, *Euro. J. Appl. Math.* **9** (1998) 417–445.
9. W. Chen, S. Conde, C. Wang, X. Wang and S. Wise, A linear energy stable scheme for a thin film model without slope selection, *J. Sci. Comput.* **52** (2012) 546–562.
10. R. Chen, G. Ji, X. Yang and H. Zhang, Decoupled energy stable schemes for phase-field vesicle membrane model, *J. Comput. Phys.* **302** (2015) 509–523.
11. Q. Cheng, X. Yang and J. Shen, Efficient and accurate numerical schemes for a hydro-dynamically coupled phase-field diblock copolymer model, *J. Comput. Phys.* **341** (2017) 44–60.
12. A. Christlieb, J. Jones, K. Promislow, B. Wetton and M. Willoughby, High accuracy solutions to energy gradient flows from material science models, *J. Comput. Phys.* **257** (2014) 192–215.
13. P. G. de Gennes, Dynamics of fluctuations and spinodal decomposition in polymer blends, *J. Chem. Phys.* **7** (1980) 4756.
14. K. R. Elder, M. Grant, N. Provatas and J. M. Kosterlitz, Sharp interface limits of phase-field models, *Phys. Rev. E.* **64** (2001) 021604.
15. C. M. Elliott and H. Garcke, Diffusional phase transitions in multicomponent systems with a concentration dependent mobility matrix, *Physica D* **109** (1997) 242–256.
16. C. M. Elliott and S. Luckhaus, A generalised diffusion equation for phase separation of a multi-component mixture with interfacial free energy, *IMA Preprint Ser.* **887** (1991) 242–256.
17. D. J. Eyre, Unconditionally gradient stable time marching the Cahn–Hilliard equation, in *Computational and Mathematical Models of Microstructural Evolution MRS Symposium Proceeding*, Vol. 529 (MRS, 1998), pp. 39–46.
18. X. Feng, Y. He and C. Liu, Analysis of finite element approximations of a phase-field model for two-phase fluids, *Math. Comput.* **76** (2007) 539–571.
19. X. Feng and A. Prol, Numerical analysis of the Allen–Cahn equation and approximation for mean curvature flows, *Numer. Math.* **94** (2003) 33–65.

20. M. G. Forest, Q. Wang and X. Yang, LCP droplet dispersions: A two-phase, diffuse-interface kinetic theory and global droplet defect predictions, *Soft Matter* **8** (2012) 9642–9660.
21. H. Garcke, B. Nestler and B. Stoth, A multiphase field concept: Numerical simulations of moving phase boundaries and multiple junctions, *SIAM J. Appl. Math.* **60** (2000) 295–315.
22. H. Garcke and B. Stinner, Second-order phase-field asymptotics for multi-component systems, *Interface Free Bound.* **8** (2006) 131–157.
23. M. E. Gurtin, D. Polignone and J. Viñals, Two-phase binary fluids and immiscible fluids described by an order parameter, *Math. Models Methods Appl. Sci.* **6** (1996) 815–831.
24. D. Han, A. Brylev, X. Yang and Z. Tan, Numerical analysis of second-order, fully discrete energy stable schemes for phase-field models of two phase incompressible flows, *J. Sci. Comput.* **70** (2016) 965–989.
25. D. Han and X. Wang, A second-order in time uniquely solvable unconditionally stable numerical schemes for Cahn–Hilliard–Navier–Stokes equation, *J. Comput. Phys.* **290** (2015) 139–156.
26. D. Jacqmin, Calculation of two-phase Navier–Stokes flows using phase-field modeling, *J. Comput. Phys.* **155** (1999) 96–127.
27. M. Kapustina, D. Tsygakov, J. Zhao, J. Wessler, X. Yang, A. Chen, N. Roach, Q. Wang T. C. Elston, K. Jacobson and M. G. Forest, Modeling the excess cell surface stored in a complex morphology of BLEB-like protrusions, *PLoS Comput. Biol.* **12** (2016) e1004841.
28. J. Kim, Phase-field models for multi-component fluid flows, *Comm. Comput. Phys.* **12** (2012) 613–661.
29. J. Kim, K. Kang and J. Lowengrub, Conservative multigrid methods for ternary Cahn–Hilliard systems, *Commun. Math. Sci.* **2** (2004) 53–77.
30. J. Kim and J. Lowengrub, Phase-field modeling and simulation of three-phase flows, *Interfaces Free Bound.* **7** (2005) 435–466.
31. H. G. Lee and J. Kim, A second-order accurate nonlinear difference scheme for the n-component Cahn–Hilliard system, *Physica A* **387** (2008) 4787–4799.
32. T. S. Little, V. Mironov, A. Nagy-Mehesz, R. Markwald, Y. Sugi, S. M. Lessner, M. A. Sutton, X. Liu, Q. Wang, X. Yang, J. O. Blanchette and M. Skiles, Engineering a 3D, biological construct: Representative research in the south carolina project for organ biofabrication, *Biofabrication* **3** (2011) 030202.
33. C. Liu and J. Shen, A phase-field model for the mixture of two incompressible fluids and its approximation by a Fourier-spectral method, *Physica D* **179** (2003) 211–228.
34. C. Liu, J. Shen and X. Yang, Decoupled energy stable schemes for a phase-field model of two-phase incompressible flows with variable density, *J. Sci. Comput.* **62** (2015) 601–622.
35. J. Lowengrub, A. Ratz and A. Voigt, Phase-field modeling of the dynamics of multicomponent vesicles spinodal decomposition coarsening budding and fission, *Phys. Rev. E* **79** (2009) 031926.
36. J. Lowengrub and L. Truskinovsky, Quasi-incompressible Cahn–Hilliard fluids and topological transitions, *Proc. Roy. Soc. Lond. Proc. Ser. A Math. Phys. Eng. Sci.* **454** (1998) 2617–2654.
37. L. Ma, R. Chen, X. Yang and H. Zhang, Numerical approximations for Allen–Cahn type phase-field model of two-phase incompressible fluids with moving contact lines, *Comm. Comput. Phys.* **21** (2017) 867–889.

38. C. Miehe, M. Hofacker and F. Welschinger, A phase-field model for rate-independent crack propagation: Robust algorithmic implementation based on operator splits, *Comput. Methods Appl. Mech. Eng.* **199** (2010) 2765–2778.
39. B. Nestler, H. Garcke and B. Stinner, Multicomponent alloy solidification: Phase-field modeling and simulations, *Phys. Rev. E* **71** (2005) 041609.
40. J. S. Rowlinson and B. Widom, *Molecular Theory of Capillarity* (Clarendon Press, 1982).
41. J. Shen, C. Wang, S. Wang and X. Wang, Second-order convex splitting schemes for gradient flows with Ehrlich–Schwoebel type energy: Application to thin film epitaxy, *SIAM J. Numer. Anal.* **50** (2012) 105–125.
42. J. Shen and X. Yang, An efficient moving mesh spectral method for the phase-field model of two-phase flows, *J. Comput. Phys.* **228** (2009) 2978–2992.
43. J. Shen and X. Yang, Energy stable schemes for Cahn–Hilliard phase-field model of two-phase incompressible flows, *Chin. Ann. Math. Ser. B* **31** (2010) 743–758.
44. J. Shen and X. Yang, Numerical approximations of Allen–Cahn and Cahn–Hilliard equations, *Discrete Contin. Dynam. Syst. A* **28** (2010) 1669–1691.
45. J. Shen and X. Yang, A phase-field model and its numerical approximation for two phase incompressible flows with different densities and viscosities, *SIAM J. Sci. Comput.* **32** (2010) 1159–1179.
46. J. Shen and X. Yang, Decoupled energy stable schemes for phase-field models of two phase complex fluids, *SIAM J. Sci. Comput.* **36** (2014) B122–B145.
47. J. Shen and X. Yang, Decoupled, energy stable schemes for phase-field models of two-phase incompressible flows, *SIAM J. Numer. Anal.* **53** (2015) 279–296.
48. J. Shen, X. Yang and Q. Wang, On mass conservation in phase-field models for binary fluids, *Comm. Compt. Phys.* **13** (2012) 1045–1065.
49. J. Shen, X. Yang and H. Yu, Efficient energy stable numerical schemes for a phase-field moving contact line model, *J. Comput. Phys.* **284** (2015) 617–630.
50. R. Spatschek, E. Brener and A. Karma, A phase-field model for rate-independent crack propagation: Robust algorithmic implementation based on operator splits, *Philos. Mag.* **91** (2010) 75–95.
51. C. Wang, X. Wang and S. M. Wise, Unconditionally stable schemes for equations of thin film epitaxy, *Discrete Contin. Dynam. Syst.* **28** (2010) 405–423.
52. C. Wang and S. M. Wise, An energy stable and convergent finite-difference scheme for the modified phase-field crystal equation, *SIAM J. Numer. Anal.* **49** (2011) 945–969.
53. C. Xu and T. Tang, Stability analysis of large time-stepping methods for epitaxial growth models, *SIAM. J. Numer. Anal.* **44** (2006) 1759–1779.
54. X. Yang, Error analysis of stabilized semi-implicit method of Allen–Cahn equation, *Discrete Contin. Dynam. Syst. B* **11** (2009) 1057–1070.
55. X. Yang, Linear, first- and second-order and unconditionally energy stable numerical schemes for the phase-field model of homopolymer blends, *J. Comput. Phys.* **327** (2016) 294–316.
56. X. Yang, J. J. Feng, C. Liu and J. Shen, Numerical simulations of jet pinching-off and drop formation using an energetic variational phase-field method, *J. Comput. Phys.* **218** (2006) 417–428.
57. X. Yang, M. G. Forest, H. Li, C. Liu, J. Shen, Q. Wang and F. Chen, Modeling and simulations of drop pinch-off from liquid crystal filaments and the leaky liquid crystal faucet immersed in viscous fluids, *J. Comput. Phys.* **236** (2013) 1–14.
58. X. Yang, G. Forest, C. Liu and J. Shen, Shear cell rupture of nematic droplets in viscous fluids, *J. Non-Newtonian Fluid Mech.* **166** (2011) 487–499.

59. X. Yang and D. Han, Linearly first- and second-order, unconditionally energy stable schemes for the phase-field crystal equation, *J. Comput. Phys.* **330** (2017) 1116–1134.
60. X. Yang and L. Ju, Efficient linear schemes with unconditionally energy stability for the phase-field elastic bending energy model, *Comput. Methods Appl. Mech. Eng.* **315** (2017) 691–712.
61. X. Yang and L. Ju, Linear and unconditionally energy stable schemes for the binary fluid-surfactant phase-field model, *Comput. Methods Appl. Mech. Eng.* **318** (2017) 1005–1029.
62. X. Yang, V. Mironov and Q. Wang, Modeling fusion of cellular aggregates in biofabrication using phase-field theories, *J. Theor. Biol.* **303** (2012) 110–118.
63. X. Yang, Y. Sun and Q. Wang, Phase-field approach for multicellular aggregate fusion in biofabrication, *J. Biol. Med. Eng.* **135** (2013) 71005.
64. X. Yang, J. Zhao and Q. Wang, Numerical approximations for the molecular beam epitaxial growth model based on the invariant energy quadratization method, *J. Comput. Phys.* **333** (2017) 104–127.
65. H. Yu and X. Yang, Numerical approximations for a phase-field moving contact line model with variable densities and viscosities, *J. Comput. Phys.* **334** (2017) 665–686.
66. P. Yue, J. Feng, C. Liu and J. Shen, Diffuse-interface simulations of drop-coalescence and retraction in viscoelastic fluids, *J. Non-Newtonian Fluid Dynam.* **129** (2005) 163–176.
67. P. Yue, J. J. Feng, C. Liu and J. Shen, A diffuse-interface method for simulating two-phase flows of complex fluids, *J. Fluid. Mech.* **515** (2004) 293–317.
68. J. Zhao, H. Li, Q. Wang and X. Yang, A linearly decoupled energy stable scheme for phase-field models of three-phase incompressible flows, *J. Sci. Comput.* **70** (2017) 1367–1389.
69. J. Zhao, Y. Shen, M. Happasalo, Z. Wang and Q. Wang, A 3D numerical study of antimicrobial persistence in heterogeneous multi-species biofilms, *J. Theor. Biol.* **392** (2016) 83–98.
70. J. Zhao and Q. Wang, A 3D hydrodynamic model for cytokinesis of eukaryotic cells, *Commun. Comput. Phys.* **19** (2016) 663–681.
71. J. Zhao, Q. Wang and X. Yang, Numerical approximations to a new phase-field model for immiscible mixtures of nematic liquid crystals and viscous fluids, *Comput. Methods Appl. Mech. Eng.* **310** (2016) 77–97.
72. J. Zhao, Q. Wang and X. Yang, Numerical approximations for a phase-field dendritic crystal growth model based on the invariant energy quadratization approach, *Int. J. Numer. Methods Eng.* **110** (2017) 279–300.
73. J. Zhao, X. Yang, Y. Gong and Q. Wang, A novel linear second-order unconditionally energy stable scheme for a hydrodynamic q-tensor model of liquid crystals, *Comput. Methods Appl. Mech. Eng.* **318** (2017) 803–825.
74. J. Zhao, X. Yang, J. Li and Q. Wang, Energy stable numerical schemes for a hydrodynamic model of nematic liquid crystals, *SIAM. J. Sci. Comput.* **38** (2016) A3264–A3290.
75. J. Zhao, X. Yang, J. Shen and Q. Wang, A decoupled energy stable scheme for a hydrodynamic phase-field model of mixtures of nematic liquid crystals and viscous fluids, *J. Comput. Phys.* **305** (2016) 539–556.
76. J. Zhu, L. Chen, J. Shen and V. Tikare, Coarsening kinetics from a variable-mobility Cahn–Hilliard equation: Application of a semi-implicit fourier spectral method, *Phys. Rev. E* **60** (1999) 3564–3572.